OAK RIDGE
NATIONAL LABORATORY
MANAGED BY UT-BATTELLE
FOR THE DEPARTMENT OF ENERGY

ORNL/TM-2013/441

Impact of HFIR LEU Conversion on Beryllium Reflector Degradation Factors

October 2013

Prepared by
Dan Ilas

UT-BATTELLE
ORNL-27 (4-00)

ORNL/TM-2013/441

Reactor and Nuclear Systems Division

IMPACT OF HFIR LEU CONVERSION ON BERYLLIUM REFLECTOR DEGRADATION FACTORS

Dan Ilas

Date Published: October 2013

Prepared by
OAK RIDGE NATIONAL LABORATORY
Oak Ridge, Tennessee 37831-6283
managed by
UT-BATTELLE, LLC
for the
U.S. DEPARTMENT OF ENERGY
under contract DE-AC05-00OR22725

CONTENTS

Page

LIST OF FIGURES

Page

LIST OF TABLES

Page

ACRONYMS AND ABBREVIATIONS

BOC	beginning of cycle
DOE	US Department of Energy
EOC	end of cycle
FP	full reactor operation power (85 MW for HEU core and 100 MW for LEU core)
HEU	highly enriched uranium
HFIR	High Flux Isotope Reactor
IRSN	Institut de Radioprotection et de Sûreté Nucléaire (Institute for Radiological Protection and Nuclear Safety)
k_{eff}	effective multiplication constant
LEU	low enriched uranium
MOC	middle of cycle (any point between BOC and EOC)
ORNL	Oak Ridge National Laboratory
PB	permanent beryllium reflector
RB	removable beryllium reflector
RNSD	Reactor and Nuclear Systems Division
RRD	Research Reactors Division
SPB	semi-permanent beryllium reflector

ACKNOWLEDGMENTS

This work was sponsored by the Global Threat Reduction Initiative, Reduced Enrichment for Research and Test Reactors Program, a program of the Nuclear National Security Administration, US Department of Energy. Review of the manuscript by David Chandler (Research Reactors Division, RRD) and Josh Peterson (Reactor and Nuclear Systems Division, RNSD), editing by Deborah Stevens (Publications) and formatting of the document by Hannah Turpin (RNSD) are very much appreciated.

ABSTRACT

An assessment of the impact of low enriched uranium (LEU) conversion on factors that may cause degradation of the beryllium reflector is performed for the High Flux Isotope Reactor (HFIR). The computational methods, models, and tools, comparisons with previous work, along with the results obtained are documented and discussed in this report.

The report documents the results for the gas and neutronic poison production and the heating in the beryllium reflector for both the highly enriched uranium (HEU) and LEU HFIR configurations, and discusses the impact that the conversion to LEU may have on these quantities.

A time-averaging procedure was developed to calculate the isotopic (gas and poison) production in the reflector. The sensitivity of this approach to different approximations is gauged and documented. The results show that gas is produced in the beryllium reflector at a total rate of 4.979 g/cycle for the HEU configuration; this rate increases by ~12% for the LEU case. The total tritium production rate in the reflector is 0.477 g/cycle for the HEU core and is approximately 11% higher for the LEU core.

A significant increase (up to ~25%) in the neutronic poison production in the reflector during operating cycles is observed for the LEU core, compared to the HEU case for regions close to the core's horizontal midplane. The poisoning level of the reflector may increase by more than two orders of magnitude during long periods of downtime.

The heating rate in the reflector is estimated to be approximately 20% lower for the LEU core than for the HEU core. This decrease is due to a significantly lower contribution from heating produced by gamma radiation for the LEU core, a benefit of using more heavy metal, with good gamma shielding properties in the LEU case.

Both the isotopic (gas and neutronic poison) production and heating rates are spatially non-uniform throughout the beryllium reflector volume. The maximum values typically occur in the removable reflector and close to the midplane.

1. INTRODUCTION

The High Flux Isotope Reactor (HFIR) is a research reactor operated at Oak Ridge National Laboratory (ORNL) that supports isotope production, material irradiation research, and neutron scattering experiments. It currently operates at 85 MW_{th} power and is fueled with highly enriched uranium (HEU) with an enrichment of 93 wt% ^{235}U. Studies are currently being conducted [1] on the conversion of HFIR's HEU core to a low-enriched uranium (LEU) core. As part of these conversion studies, the impact of the higher power (100 MW_{th}) of the LEU core and spectral differences was analyzed for the irradiation locations [2]. This study revealed that the beryllium reflector with the LEU core may see both a more intense neutron flux and a different spectrum than that with the HEU core. The differences observed for the irradiation locations indicated a potential impact of the LEU conversion on the gas production and heating in the beryllium reflector. The gas accumulation, neutronic poison buildup, and heating in the beryllium reflector will be collectively referred to as beryllium degradation factors in this report. The first two factors, gas and neutronic poison accumulation, will together be referred to as isotopic production. The study presented in this report compares beryllium degradation factors for the current HEU-fueled HFIR and the envisioned LEU configuration.

Gas accumulation and heating in metallic beryllium were recognized to lead to embrittlement, swelling and potential cracking of beryllium, and to affect its thermal conductivity properties. Earlier studies, both experimental and theoretical, that were performed in support of fusion programs [3, 4] showed that the swelling is a function of the neutron fluence in the material. Accumulation of microvoids and bubbles in beryllium can lead to cracking with the release of tritium, a radioactive gas with a half-life of just over 12 years. Although the radioactivity of tritium consists in the emission of low-energy beta particles, it may constitute an occupational hazard when ingested because it can enter the body's metabolism; the tritium atom is chemically identical to the hydrogen atom.

A previous ORNL study on nuclear gas production and heating of the beryllium reflector in the HFIR reactor was conducted in 1995 in relation to a reflector redesign [5]. The heating studies were necessary at that time to assess the thermal stresses that occur in the beryllium.

More recently, other studies estimated the amount of thermal poison buildup in the HFIR beryllium reflector in order to more accurately predict reactivity worth at startup after a long reactor shutdown period [6], [7]. The procedure used the ORIGEN module of the SCALE package [8] to estimate the total amount of ^{3}He and ^{6}Li produced in the reactor as a function of time.

The computational methods and models used in the current study are documented in Section 2 of this report. Isotopic production analytical methods and studies on the sensitivity of the results to different approximations, as well as the methodology used to estimate gas production, are presented in Section 3. The model and methodology used to compute heating in the beryllium reflector are described in Section 4. Results obtained using these methods for both the HEU and the designed LEU cores are presented and compared in Section 5. Concluding remarks are provided in Section 6.

2. GEOMETRY AND COMPUTATIONAL MODELS

2.1 CODES AND METHODS

As in previous HEU-LEU comparison studies [2], enhanced HEU models based on the Cycle 400 HEU model of the HFIR fresh core [1, 9] and the 2011 model for the LEU core [1] have been used. These models use homogenized fuel regions* and therefore do not take into account the fine structure and distribution of the fuel in the fuel plates. The fueled regions are modeled by volumetrically homogenizing the fuel meat, filler, clad, and water coolant. To account for the non-uniform fuel meat thickness along the involute fuel plates, they are divided into several radial regions with different spatially-averaged fuel concentrations.

The neutron-photon-electron Monte Carlo transport code MCNP5.1.51 [10] is used in this study to perform neutronic and/or coupled neutron-gamma calculations for the quantities of interest. The transport calculations typically used ENDF/B VII.0 cross section libraries. However, when a certain isotope in ENDF/B VII.0 did not contain gamma production data, other cross-section libraries were used.

Besides the beginning-of-cycle (BOC) fresh fuel models, the middle-of-cycle (MOC) and the end-of-cycle (EOC) computational models were obtained based on previous depletion studies performed with VESTA [11]. The BOC, MOC, and EOC models for both the HEU and LEU cores were further enhanced by adding the necessary surface, cell and material cards, as well as the tally cards to calculate the target quantities on the desired spatial grid. The MCNP tally results were further used in analytical models to calculate the desired responses, as described in this report. These calculations were typically performed in a Microsoft EXCEL™ spreadsheet.

The main results (isotopic production, energy deposition) depend on MCNP-calculated quantities (reaction rates, heating tallies) integrated over the entire energy domain and over relatively large spatial regions. Because of the estimative scope of this study, the tally regions in the MCNP model were chosen large enough, so that the relative statistical errors obtained using a few hours of runtime on a computer cluster for the reaction rates or heating tallies were typically well below 1%, with somewhat larger values (between 1% and 2%) at the outer edge of the permanent reflector. Given these considerations, no special variance reduction techniques have been employed in this study.

2.2 GEOMETRY MODELS

The beryllium reflector in HFIR consists of a series of concentric annuli (Fig. 1) located outside the fuel and control element regions. The computational models account for the physical separation of the beryllium reflector into three annuli (removable – RB, semipermanent – SPB, and permanent – PB). For computational purposes, these three annuli are also divided radially into 3, 1, and 7 rings, respectively. Axially, the MCNP beryllium reflector model was enhanced to consist of 12 zones symmetrically distributed above and below the horizontal midplane of the reactor.

* Preliminary calculations with a detailed MCNP model that explicitly models the geometry of the fuel elements in the LEU core show significant differences in the cycle length (~20% longer) between this model and the homogenized model.

Throughout the rest of this report, the following terminology will be used.

- "Zone" refers to an axial mesh of reflector between two consecutive horizontal planes.
- "Ring" refers to the radial mesh: a cylindrical shell of beryllium reflector that spans axially from the top to the bottom of the reflector.
- "Region" refers to a zone within a certain ring and is the smallest unit (two-dimensional spatial mesh) for which evaluations were performed.

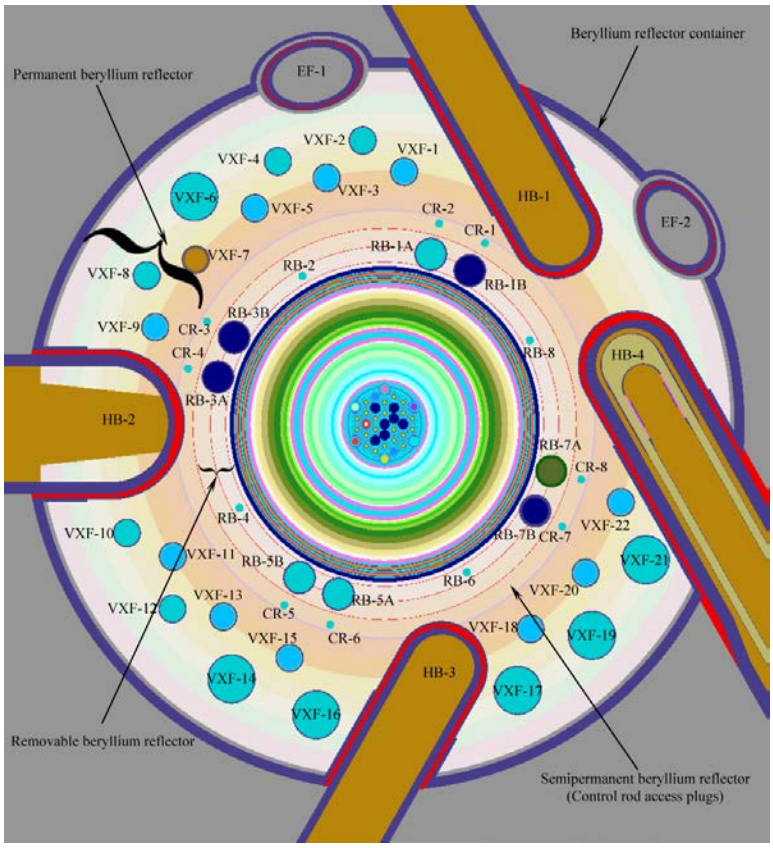

Fig. 1. HFIR schematic at core midplane (from [12]).

Table 1 shows the inner and outer radii of the computational rings in the beryllium reflector MCNP model. Note that the first five rings have gaps between their common radial boundaries. These gaps model the grooves between different sections of the reflector, and are filled with water.

Table 1. Boundaries of the rings in the beryllium reflector MCNP model

Annulus	Ring #	R_i (cm)	R_o (cm)
Removable reflector	1	24.4475	25.0825
	2	25.15108	27.46375
	3	27.53233	30.25267
Semipermanent reflector	4	30.32125	33.02
Permanent reflector	5	33.3375	36.3375
	6	36.3375	39.3375
	7	39.3375	42.3375
	8	42.3375	45.3375
	9	45.3375	48.3375
	10	48.3375	51.3375
	11	51.3375	54.61

The axial zones are generally equal in height, 5 cm each, and are symmetrically distributed with respect to the midplane. The only exceptions are the top and bottom regions, which have been enlarged to match the top and bottom boundaries of the reflector at z = ±30.48 cm; each of these regions has a height of 5.48 cm. Table 2 shows the boundaries of the 12 axial zones.

The 11 radial rings and 12 axial zones result in a total of 11×12 = 132 regions, which are numbered consecutively from 1 to 132, with each consecutive grouping of 12 regions corresponding to the same ring (i.e., regions 1 to 12 correspond to the axial zones from top to bottom inside the first ring, regions 13 to 24 to the second ring, etc.). The R-Z meshing just described neglects any azimuthal dependence of the degradation factors; the azimuthal dependence is smeared over an entire ring. Therefore, the results represent azimuthally homogenized quantities.

Figure Fig. 2 shows a schematic R-Z layout and numbering for the regions in the beryllium reflector.

The volumes for each of the regions defined in the reflector were estimated statistically with MCNP and are shown graphically in Fig. 3. The differences in the magnitude of the volumes for each region located within the same ring are in general explained by different intrusions of the horizontal beam tubes into the reflector, around its midplane. The plot shown in Fig. 3 will be typically used for presenting the space-dependent results throughout this study. This allows for a concise presentation of a two-dimensional (R-Z) information onto a one-dimensional plot. It can also be interpreted as 11 plots next to each other, with the 11 plots containing 12 points each, with each point corresponding to a zone within a certain ring (certain radial range) of the reflector.

Table 2. Boundaries of the zones in the beryllium reflector MCNP model

Zone #	Z_{top} (cm)	Z_{bottom} (cm)
1	30.48	25
2	25	20
3	20	15
4	15	10
5	10	5
6	5	0
7	0	-5
8	-5	-10
9	-10	-15
10	-15	-20
11	-20	-25
12	-25	-30.48

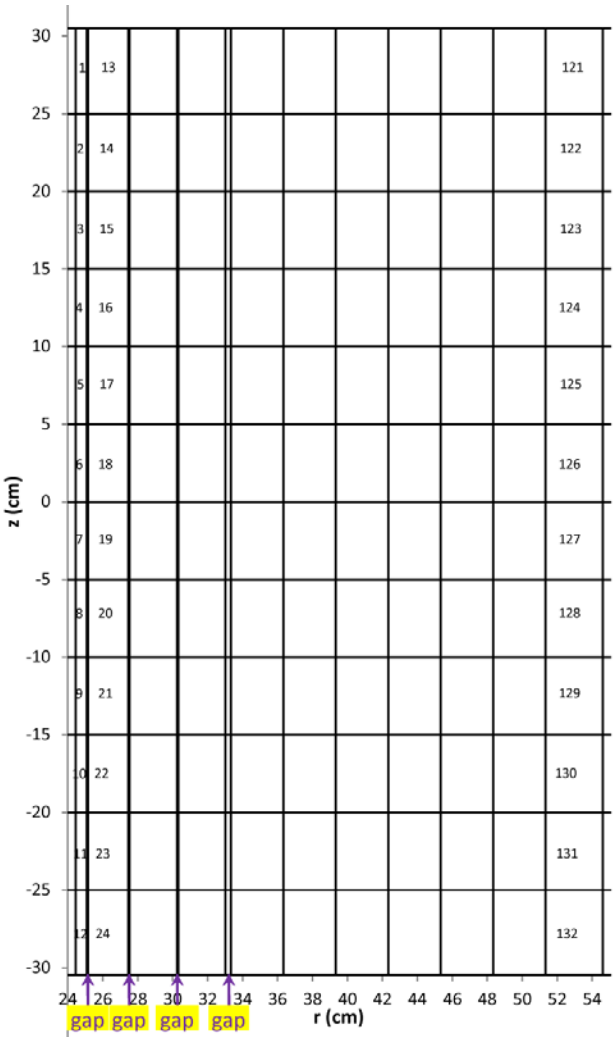

Fig. 2. Schematic R-Z view of the HFIR's beryllium reflector and region numbering for this study.

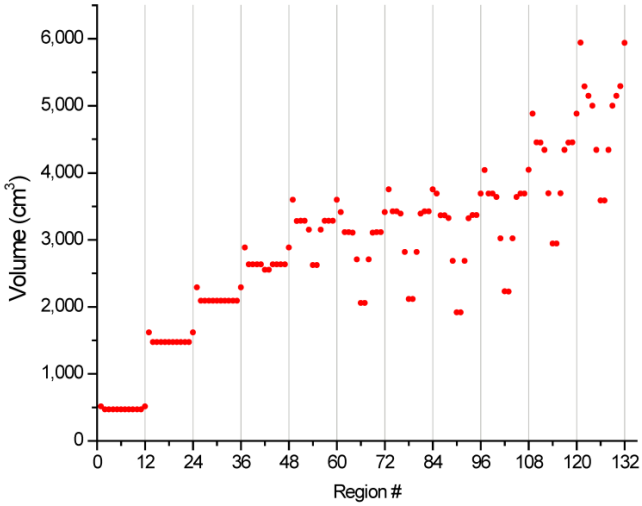

Fig. 3. Distribution of volumes for the 132 regions in the HFIR beryllium reflector.

3. GAS PRODUCTION MODEL

3.1 DERIVATION OF GAS PRODUCTION EQUATIONS

With standard notations (^3T stands for tritium), the following nuclear reactions are considered (intermediate steps leading to short-lived isotopes such as ^6He and ^8Be are omitted):

$$^9Be + n \rightarrow {}^6Li + \alpha \quad (1)$$

$$^9Be + n \rightarrow 2\alpha + 2n \quad (2)$$

$$^9Be + \gamma \rightarrow 2\alpha + n \quad (3)$$

$$^6Li + n \rightarrow {}^3T + \alpha \quad (4)$$

$$^3T \xrightarrow{\beta^-} {}^3He \quad (5)$$

$$^3He + n \rightarrow {}^3T + p \quad (6)$$

The reactions represented by Eqs. (1–3) are the initiating reactions for gas production in the beryllium reflector. Other neutronic reactions are possible, but their probability is too low to have an impact on this study, given the neutron spectra typical of the HFIR's beryllium reflector. Also, with the exception noted later, the photo-neutronic reaction on ^9Be (Eq. 3) may be neglected as a contributor to the gas production. As shown in Fig. 4, the cross section for this reaction is two to three orders of magnitude smaller than the cross sections associated with the neutronic channels. Because the neutron spectrum and the gamma spectrum are changing in different ways with the depth in the beryllium reflector, it is possible that in certain regions of the beryllium reflector the fast-neutron flux decreases significantly and the gamma channel starts to compete with the neutronic channel. This phenomenon will be explained in more detail in section 3.6.

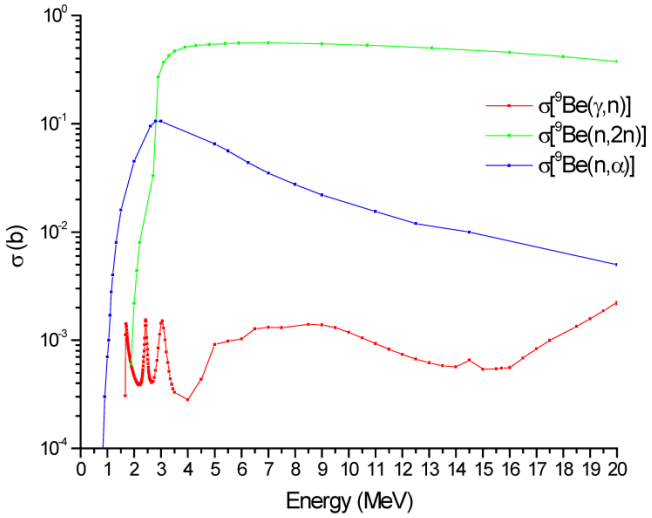

Fig. 4. Energy dependence of the initiating gas production ENDF/B-VII cross sections.

Based on the above reactions, the following balance equations can be written:

$$\frac{dB}{dt} = -\left(\sigma_B + \sigma_{2n}\right)\Phi B - \sigma_\gamma \Phi_\gamma B \tag{7}$$

$$\frac{dL}{dt} = \sigma_B \Phi B - \sigma_L \Phi L \tag{8}$$

$$\frac{dT}{dt} = \sigma_L \Phi L - \lambda T + \sigma_H \Phi H \tag{9}$$

$$\frac{dH}{dt} = \lambda T - \sigma_H \Phi H \tag{10}$$

$$\frac{d\alpha}{dt} = \left(\sigma_B + 2\sigma_{2n}\right)\Phi B + 2\sigma_\gamma \Phi_\gamma B + \sigma_L \Phi L \tag{11}$$

In Eqs. (7-11), *B, L, T, H,* and α are functions of time and represent the number of atoms per cm^3 of ^9Be, ^6Li, ^3T, ^3He, and α particles, respectively, while Φ and Φ_γ are the neutron and gamma fluxes, respectively. The cross sections σ_B, σ_{2n}, σ_γ, σ_L, σ_H correspond to the $^9Be(n,\alpha)$, $^9Be(n,2n)$, $^9Be(\gamma,n)$, $^6Li(n,\alpha)$, and $^3He(n,p)$ reactions, and λ is the decay constant for the β^- decay of ^3T. The products $r_B \equiv \sigma_B\Phi$, $r_{2n} \equiv \sigma_{2n}\Phi$, $r_\gamma \equiv \sigma_\gamma\Phi_\gamma$, $r_L \equiv \sigma_L\Phi$, $r_H \equiv \sigma_H\Phi$ represent the reaction rates for the process described by the respective cross sections.

Analytical solutions to Eqs. (7–11) were used in the 1995 ORNL study [5] to assess the amount of gas produced in the reflector. The solutions in that study were obtained using the Laplace transform technique. The analytical solutions listed below, which will be used throughout this study, are obtained using direct integration of Eqs. (7–11).

With B_0 as the initial concentration of beryllium and setting $r_1 \equiv r_B + r_{2n} + r_\gamma$, Eq. (7) can be integrated to obtain

$$B(t) = B_0 e^{-r_1 t}. \tag{12}$$

Using the solution of Eq. (12) in Eq. (8) and integrating gives the time behavior of the ^6Li concentration:

$$L(t) = \frac{r_B B_0}{r_L - r_1} e^{-r_1 t} + \left(L_0 - \frac{r_B B_0}{r_L - r_1} \right) e^{-r_L t}. \tag{13}$$

To obtain the tritium concentration, we first make the observation that the ^3He concentration is small during steady state reactor operation when compared to the tritium concentration, and therefore, a

good approximation is $T(t) \cong T(t) + H(t)$. Adding together Eqs. (9) and (10), we obtain the following simpler equation, which can be easily integrated:

$$\frac{d(T+H)}{dt} = \sigma_L \Phi L \ . \tag{14}$$

Using Eq. (13) in Eq. (14), the latter has the following solution:

$$T(t)+H(t) = \frac{r_B B_0}{r_1}\left(1 - \frac{r_L}{r_L - r_1}e^{-r_1 t} + \frac{r_1}{r_L - r_1}e^{-r_L t}\right) + L_0\left(1 - e^{-r_L t}\right) + T_0 + H_0 . \tag{15}$$

Equation (10) can be rewritten as

$$\frac{dH}{dt} = \lambda(T+H) - (\lambda + r_H)H \ . \tag{16}$$

Making use of Eq. (15) in Eq. (16), the solution to Eq. (16) is

$$H(t) = \frac{\lambda r_B B_0}{r_1}\left(\frac{1-e^{-(\lambda+r_H)t}}{\lambda + r_H} + \frac{r_L}{r_L - r_1}\frac{e^{-r_1 t}}{r_1 - (\lambda + r_H)} - \frac{r_1}{r_L - r_1}\frac{e^{-r_L t}}{r_L - (\lambda + r_H)} + \frac{(r_L + r_1 - (\lambda + r_H))e^{-(\lambda+r_H)t}}{(r_L - (\lambda + r_H))(r_1 - (\lambda + r_H))}\right) + \tag{17}$$
$$\lambda L_0\left(\frac{1-e^{-(\lambda+r_H)t}}{\lambda + r_H} + \frac{e^{-r_L t}}{r_L - (\lambda + r_H)} - \frac{e^{-(\lambda+r_H)t}}{r_L - (\lambda + r_H)}\right) + \frac{\lambda T_0}{\lambda + r_H} + \lambda H_0\left(\frac{1-e^{-(\lambda+r_H)t}}{\lambda + r_H} + \frac{e^{-(\lambda+r_H)t}}{\lambda}\right)$$

While Eq. (15) itself provides a way to estimate the tritium concentration with a good approximation by setting the ^3He concentration to zero, it might be less accurate during long reactor shutdown periods. From Eqs. (15) and (17), *T(t)* can be calculated exactly as

$$T(t) = (T(t) + H(t)) - H(t). \tag{18}$$

Finally, making use of Eqs. (12) and (13) in Eq. (11), the helium concentration can be calculated as

$$\alpha(t) = B_0\left(2\left(1 - e^{-r_1 t}\right) - \frac{r_B}{r_L - r_1}\left(e^{-r_1 t} - e^{-r_L t}\right)\right) + L_0\left(1 - e^{-r_L t}\right) + \alpha_0 . \tag{19}$$

An analytical solution for the gas production equations permits convenient parametric studies, even using a spreadsheet. This provides an alternative to using a code such as ORIGEN to burn the beryllium. To use the analytical equations, the reaction rates must be known; they can be obtained through an MCNP calculation.

The energy dependence represented in Fig. 4 for the cross sections of the reactions described by Eqs. (1–3) shows that the initiating reactions become significant at incident particle energies beyond 1 MeV. This means that the conditions for higher gas production are created in regions where the fast-neutron flux is higher, such as in the removable reflector. Low-energy neutronic channels exist for gas production also, such as the $^3T/^3He$ production and the α production that originate from ^6Li. However, unless this ^6Li isotope already exists (such as an impurity), it must be produced via the $^9Be(n,\alpha)$ reaction, and therefore it is also produced via a fast-neutron reaction channel.

Although ^{3}He is a gas, its production is expected to be negligible relative to other gases, and therefore it is not of concern from the gas production standpoint. However, monitoring ^{3}He, as well as ^{6}Li, is important because these isotopes are strong thermal neutron absorbers and could potentially lead to degradation of the beryllium properties as a neutron reflector.

Because the neutronic cross sections for reactions described by balance Eqs. (1–6) are one-group cross sections, they embed the neutron (or gamma) spectral information. Therefore, their value is expected to change at different points in the reflector and at different times during the operation as the spectral information changes. The neutron flux can also change from point to point in the reflector and also with time. Based on these considerations, a number of challenges have been identified and are analyzed and discussed in the following sections.

3.2 INTRA-CYCLE TIME DEPENDENCE OF CORE ISOTOPICS

Because of the core depletion and fission product buildup, both the neutron fluxes and the reaction cross sections change over time during any given irradiation cycle (HFIR operation at full power). To quantify the effect, the differences in the one-energy-group neutron fluxes and the cross sections weighted with the spectra at BOC and EOC for the HEU core are calculated as (EOC-BOC)/BOC and are shown on the left in Fig. 5. It can be seen that the difference in the fluxes is greater at the top and bottom of the reflector, decreases at the midplane, and also decreases deeper (away from the core) in the reflector. The decrease with the depth in the reflector is also seen for the differences in cross sections. The near overlapping of the differences for the cross sections in the two reactions on beryllium can be seen, as well as the overlapping for the reactions on lithium-6 and helium-3. This reflects the sensitivity of each pair of reactions to the fast spectrum and the thermal spectrum, respectively. The differences between the EOC and the BOC reaction rates, shown on the right in Fig. 5, are seen to be substantial, especially for the thermal reactions. It is remarkable that these differences reach a minimum for regions situated near the reactor horizontal midplane. This indicates that the gas production in the beryllium reflector at regions near this midplane is not very sensitive to the model used.

The latter statement can be confirmed by analyzing the helium-4 (alpha particles) and the tritium production calculated with reaction rates obtained with either the BOC or the EOC models. Consider the hypothetical case where the irradiation takes place for 17 cycles, 25 days long each, with either the BOC or the EOC neutron fluxes and spectra (the 17 cycles are simulated continuously, with zero downtime between them). The differences shown in Fig. 6 demonstrate the insensitivity of the gas production on the core model at midplane and the larger impact the model chosen may have on the results for the top and bottom regions of the reflector. In particular, using a fresh-fuel BOC model for the whole irradiation cycle leads to an underestimation of the gas production and an overestimation of the neutronic poison production.

Although the analyses in this section were performed for the HEU core, the trends also hold true for the LEU core.

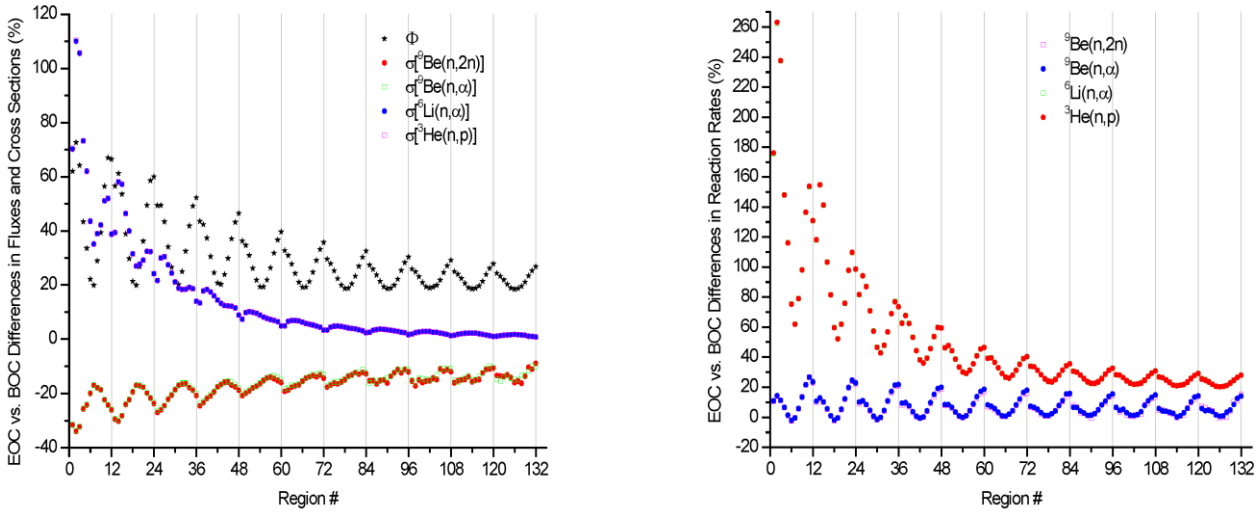

Fig. 5. Differences in fluxes and cross sections (left) and in reaction rates (right) for BOC and EOC of the HEU core.

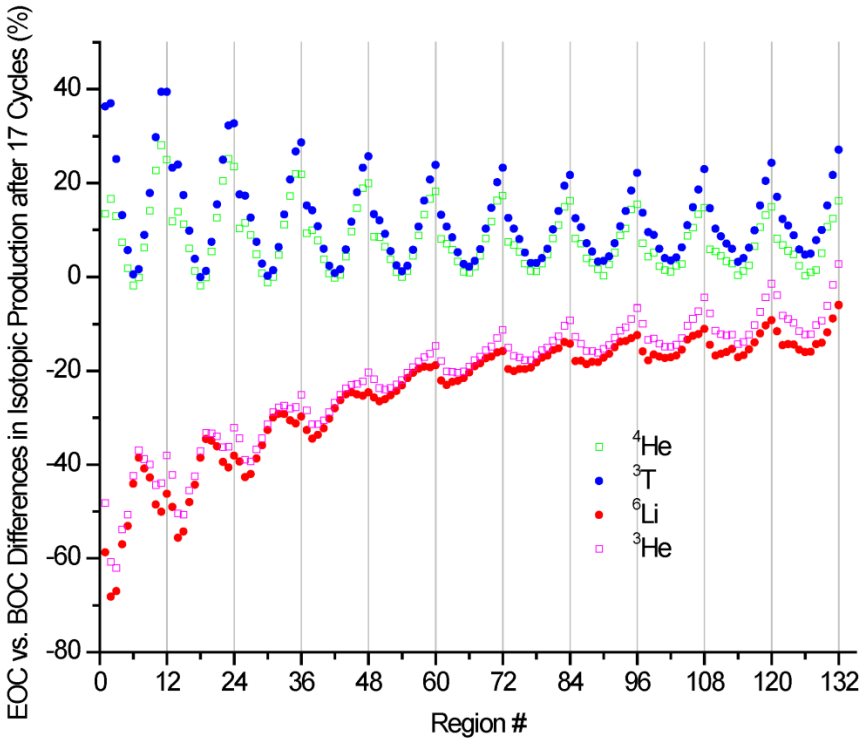

Fig. 6. Differences in isotopic production in beryllium reflector after 17 irradiation cycles with BOC and EOC reaction rates for the HEU core.

3.3 INTRA-CYCLE CONTROL ELEMENTS MOVEMENT

During reactor operation, the control elements are moved vertically to maintain the reactor's critical state. Due to this movement, the fluxes in different parts of the reflector and the reaction cross sections in these regions vary during an operating cycle. FigureFig. 7, reproduced from Reference [1], shows the position of the black (Eu_2O_3-Al) lower boundary of the outer control element relative to the bottom of the fuel plates at different times during the reactor cycle. The inner control element moves symmetrically relative to the outer element in the opposite direction, below the reactor midplane, during the reactor operation. The movement of the two control elements thus creates an opening for the thermal neutrons to easily reach the reflector around the reactor midplane, and this opening increases as the reactor cycle progresses towards the EOC. The opening has a lesser impact on the fast component of the neutron flux, but it effectively creates a window for the thermal neutron current impinging upon the reflector from the active core, thus impacting the thermal reactions on ^{6}Li and ^{3}He. During an operating cycle, the opening created by the control elements increases, faster at the beginning, immediately after the BOC, to compensate for the xenon buildup, and then slower towards the EOC.

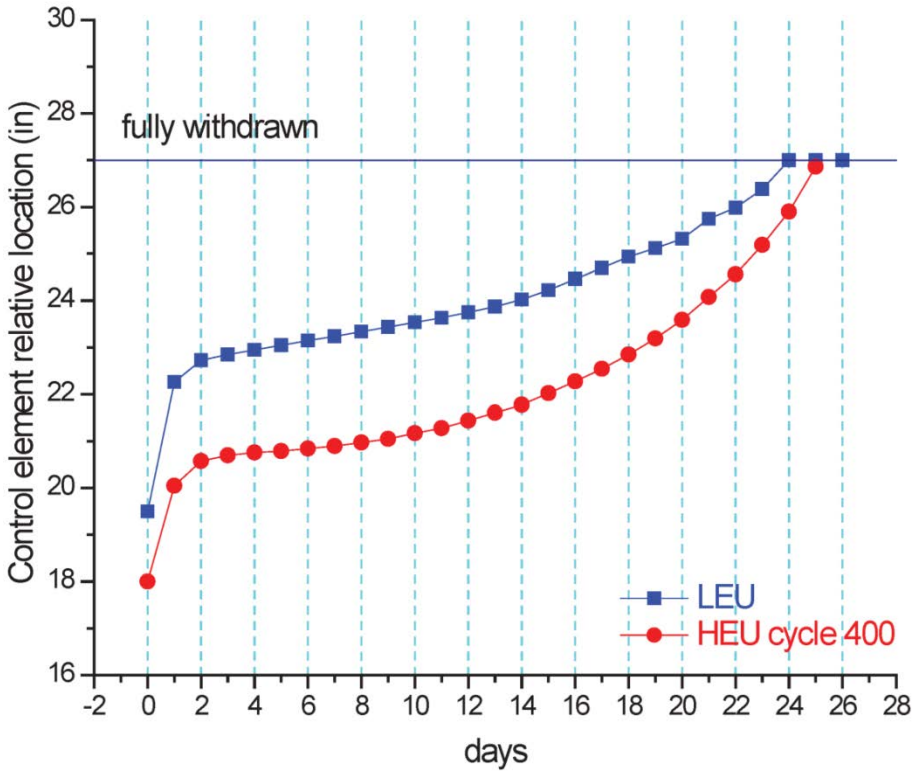

Fig. 7. Outer control element position during the irradiation cycle (from [1]).

To account for the moving parts during the reactor operation, we assert that the best model is to use time-averaged values for the reaction rates. The time averaging is performed by estimating the reaction rates at different times during the irradiation cycle, in particular every 5 days, and taking a time average over the cycle length. This means that a time-averaged reaction rate R is calculated as

$$R = \frac{2.5 \times R_{BOC} + 5 \times R_{MOC\_05} + 5 \times R_{MOC\_10} + 5 \times R_{MOC\_15} + 5 \times R_{MOC\_20} + 2.5 \times R_{EOC}}{25}, \quad (20)$$

where R_{BOC}, R_{MOC_n}, and R_{EOC} are the reaction rates at BOC, MOC *n* days into the cycle, and EOC, respectively.

The time-averaging described above accounts for both changes in the geometry of the HFIR model and changes in the isotopics of the core described in Section 3.2. An alternative to using this time-averaging procedure is to use a unique set of reaction rates, say at 10 days into the cycle. To assess the magnitude of the effect due to the control elements opening during an irradiation cycle, Fig. 8 shows the differences expected in the isotopic production in beryllium after 17 cycles of continuous irradiation with the MOC_10 model and the time-averaged model for the HEU core. The largest impact observed due to the model occurs in regions radially close to the core (removable reflector) and axially away from the midplane. These trends should also be valid for the LEU core, perhaps with a different magnitude.

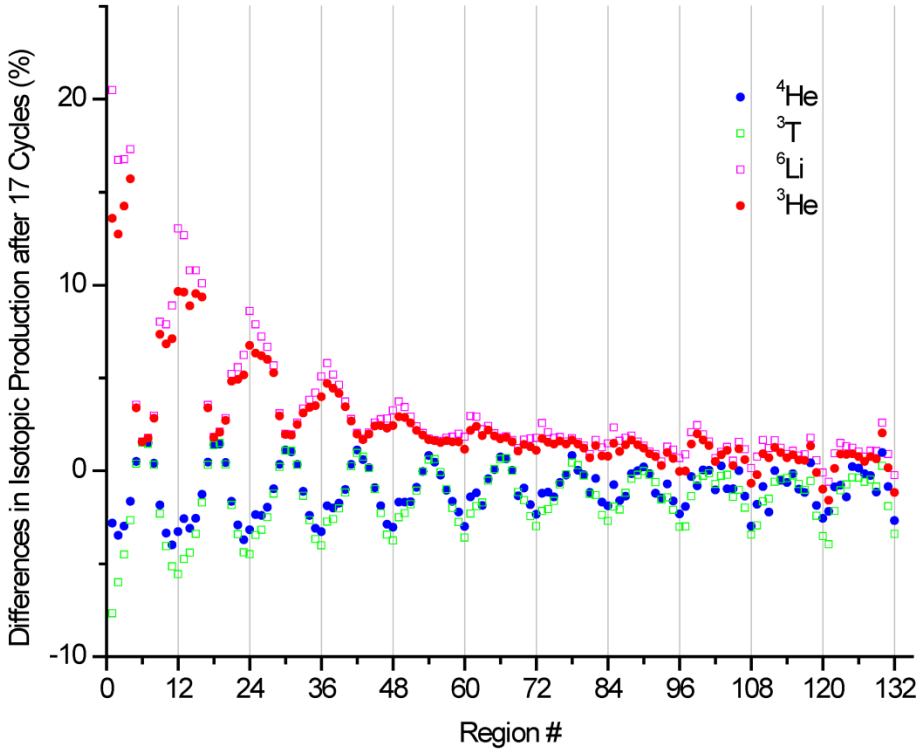

Fig. 8. Differences in isotopic production in beryllium reflector after 17 irradiation cycles with 10-day and time-averaged reaction rates for the HEU core.

3.4 NEUTRON POISON BUILDUP

Because of the buildup of the neutron poisons ^{6}Li and ^{3}He in the beryllium reflector during irradiation, the neutron fluxes and the reaction cross sections change from one cycle to the next. To assess the impact of neutron poison buildup in HFIR's beryllium reflector during irradiation, a model containing the maximum concentrations of ^{6}Li and ^{3}He in each ring of the reflector was built for the BOC core (the "maximum poisoned model"). These concentrations correspond to the maximum

values for the irradiation of the removable, semipermanent, and permanent reflector. This “maximum poisoned model” is a hypothetical model, corresponding to the unlikely event when the three types of reflector are simultaneously reaching their respective end of life.

The isotopic production after 17 irradiation cycles* obtained with fluxes and cross sections from this model were compared with the isotopic production from the reference model that uses the standard Cycle 400 BOC concentrations of ^{6}Li and ^{3}He. FigureFig. 9 shows the differences in the isotope concentrations at the end of 17 25-day cycles of continuous irradiation time. The differences are observed to be small, especially for the semipermanent and permanent reflectors, and the impact on gas production is close to zero. The larger differences for the production of ^{6}Li and ^{3}He isotopes in the removable reflector are due to the fact that the standard model for Cycle 400 uses fresh composition for the removable reflector, whereas the maximum poisoned model starts out with an accumulation of ^{6}Li and ^{3}He in the removable reflector that corresponds to 40 cycles of irradiation (the design lifetime of this reflector).

This low sensitivity of the gas production to the initial amount of neutronic poisons in the reflector provides the grounds for justifying use of the standard Cycle 400 model for the HEU model and its corresponding LEU model throughout this study, with little concern regarding the errors in the calculation of the amount of gas produced.

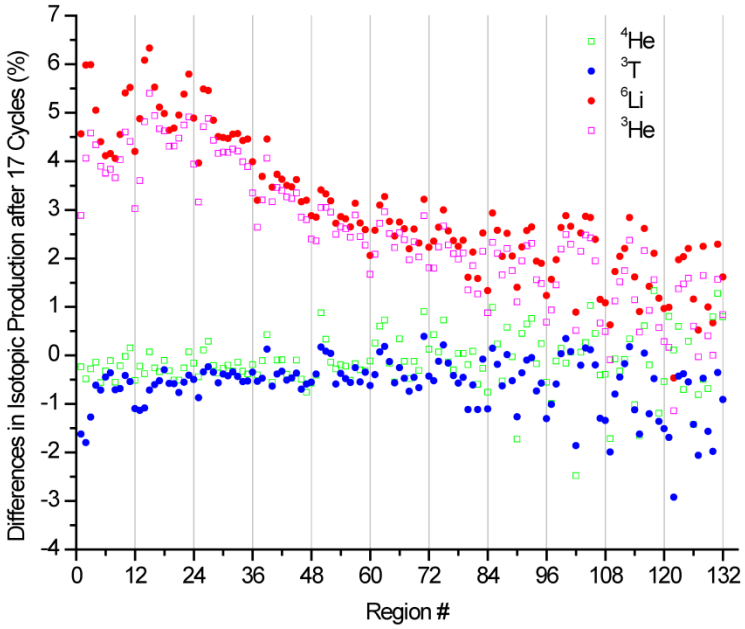

Fig. 9. Differences in isotopic production prediction in beryllium reflector after 17 irradiation cycles with maximum poisoned and standard BOC models for the HEU core.

* Most of the time, using 17 cycles for the examples in this study does not have any particular significance. The 17 cycles are the approximate age of the SPB and PB reflectors at the start of cycle 400. This irradiation time is also long enough for all of the quantities to reach an equilibrium behavior.

3.5 IRRADIATION HISTORY

The irradiation history of HFIR's beryllium reflector follows the operational cycles of the reactor. This includes a succession of irradiation periods ("cycles"), each up to about 26 days long, followed by periods of downtime that vary in duration. To assess the impact the irradiation history might have upon the gas production in beryllium, we simulated a succession of 25-day-long full-power operational cycles each followed by a 25-day downtime period. This constitutes the "detailed model." Results obtained with the detailed model were compared to the results obtained after an equivalent duration of continuous irradiation ("simplified model"). The averaging procedure described by Eq. (20) was used in both the detailed and simplified models, and the irradiation was followed for 17 irradiation cycles. The isotopic production after this irradiation time was compared with the two models for the HEU core, with the detailed model as reference; the differences are plotted in Fig. 10.

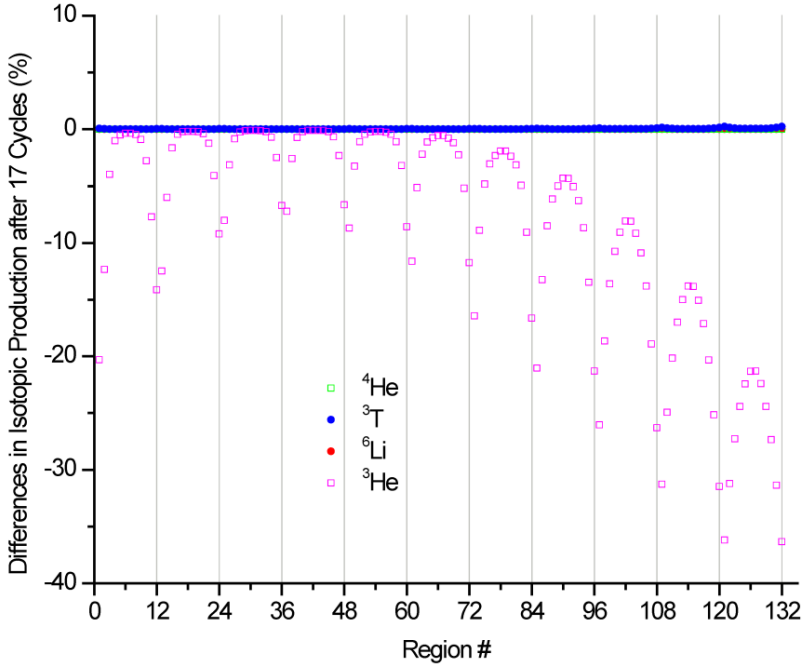

Fig. 10. Differences in isotopic production prediction in the beryllium reflector after 17 irradiation cycles with detailed and simplified time-averaged models for the HEU core.

With the noticeable exception of ^{3}He, the differences in prediction given by the two models are practically zero. For ^{3}He, the difference is larger in regions away from the midplane and deeper into the reflector; the simplified model always underestimates the production. One explanation for the underestimation is that tritium does not have as long a time to decay in this scenario as it does when a downtime is present between cycles. The difference in ^{3}He, however, does not affect the total gas production predicted by the two models because the fraction of ^{3}He in the total gas production is negligible. A similar behavior was observed for the LEU models. Note that while the irradiation time is the same, that is, 17 cycles × 25 days = 425 days of total irradiation, the corresponding energy produced by the reactor is different in the HEU and LEU models due to the different nominal full power of the reactor envisioned for the two cores: 36,125 MWd for the HEU core vs. 42,500 MWd for the LEU core.

3.6 GAS PRODUCTION BY GAMMA RADIATION

All of the discussion so far has focused on the gas production due to neutronic reactions in beryllium. Equation (3), however, suggests that gamma irradiation of the beryllium could also produce helium via a photoneutron reaction. FigureFig. 4 indicates that this effect is small, given that the cross section for the photoneutronic reaction, which is nonzero for incident energies of the gamma radiation beyond ~1.6 MeV, is two to three orders of magnitude lower than the cross section for the neutron reactions. This holds true if the neutron and gamma fluxes are comparable in magnitude. More precisely, it is the magnitude of the fast component of the neutron flux and component of the gamma spectrum beyond ~1.6 MeV that matters. The good neutron thermalizing property of the beryllium reflector means that conditions may exist for a reduced fast-neutron component deep in the reflector. The gamma spectrum, however, is less affected by collisions with the beryllium atoms and therefore does not degrade (becoming softer) with radial distance in the reflector as quickly as the neutron spectrum.

With the above arguments, conditions for gamma radiation to have an impact on the gas production may exist deeper into the permanent beryllium reflector. To assess this assertion, the neutron and gamma spectra were each tallied in 238 energy groups on an energy grid typical of the 238-group SCALE library for two regions in the beryllium permanent reflector near the midplane: one region in the innermost ring of the permanent reflector (ring 5), and one in ring 11, the outermost ring (Figure 11). Comparisons between the gamma and the neutron spectra show that the relative ratio of the two varies between about 10 and 100 with radial distance through the reflector for the energy range of interest. This indicates that the photoneutron reaction rates can become competitive in magnitude with the neutronic reaction rates in the beryllium reflector with the relative ratio increasing from ~0.01 to ~0.1 from the innermost to the outermost regions of the permanent reflector and therefore the gas production due to the gamma radiation may add a few percent to the total gas production in the permanent reflector.

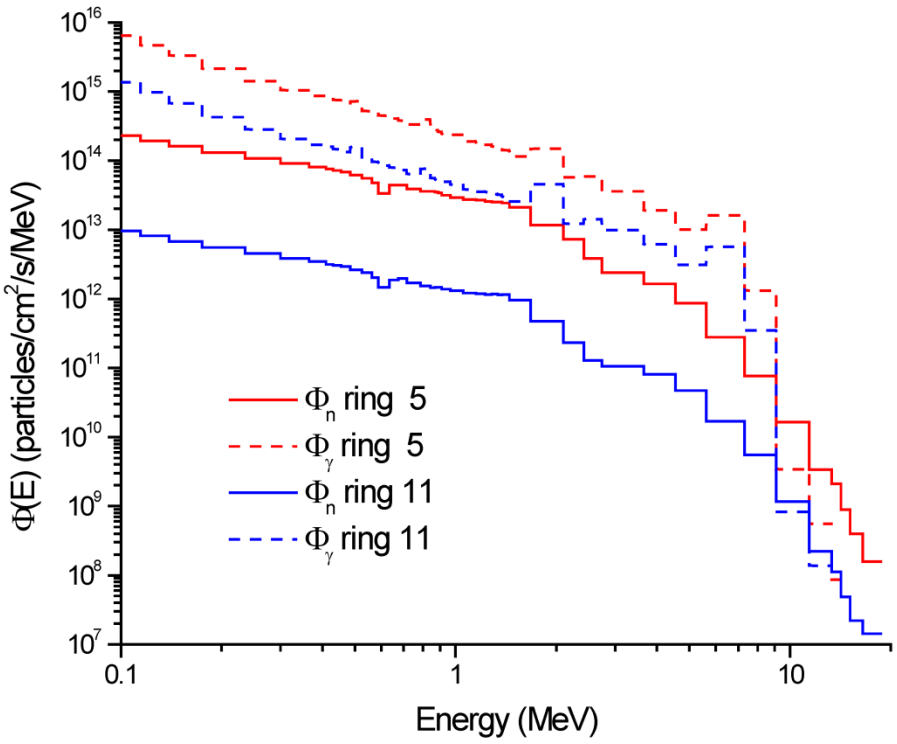

Fig. 11. Neutron and gamma spectra in the innermost and outermost rings of the permanent beryllium reflector near the midplane.

3.7 INTRINSIC SPATIAL VARIATION

Both the neutron fluxes and spectral information (therefore the cross sections) vary spatially in the reflector due to intrinsic geometric factors (distance from the source). For example, the magnitude of the flux varies inversely proportional to some power of the distance from the source to the point of detection (or point of interest, in general).

For an adequate spatial representation of the isotopic concentration distributions, a detailed meshing of the reflector in 132 regions was implemented, as described earlier in Section 2.2, and region-wise gas production values were calculated in each region. This meshing allows (r,z) space dependence evaluations for the gas production with adequate precision for the scope of this study. The region-wise isotopic production map on this 2-D mesh (R-Z) is illustrated in Fig. 12, where results corresponding to 17 cycles of continuous irradiation for the HEU core are shown in the format described in Section 2.2.

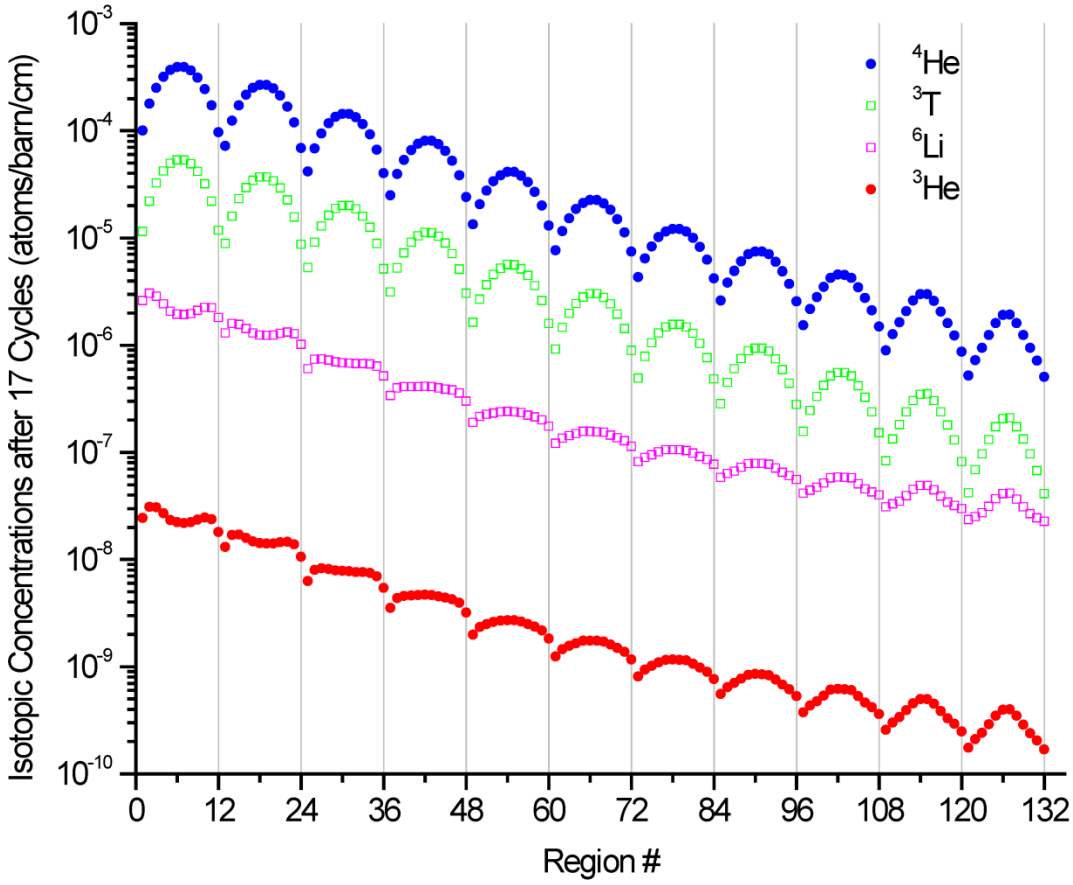

Fig. 12. Isotopic concentrations after 17 cycles of continuous irradiation in the HEU core.

3.8 METHODOLOGY

Based on the discussion above, the methodology for assessing gas production after a number of cycles includes the following steps:

1. Run MCNP simulations for the HFIR HEU configuration ("configuration" meaning certain control elements position and fuel composition) at a number of times in an operating cycle and tally the reaction rates for the reactions of interest for gas production. In particular, we chose six times, including BOC and EOC states, each 5 days apart. The cycle was always considered to be 25 days long.

2. Collect the reaction rates for each of the six simulations and normalize appropriately to obtain instantaneous reaction rates at each of the six times. The reaction rates are normalized to the neutron source:

$$S = \frac{\bar{\nu} P}{\bar{\varepsilon} k_{eff}}, \tag{21}$$

where $\bar{\nu}$ is the average number of neutrons released per fission, P is the reactor power (85 MW for HEU and 100 MW for LEU), $\bar{\varepsilon}$ is the useful energy released per fission (200 MeV),

and k_{eff} is the effective multiplication factor provided by MCNP (always very close to 1.0 during the reactor's operation). Because all of these quantities are relatively constant during operation, the neutron source also does not change significantly and is considered constant for each of the HEU or LEU cores.

3. Calculate average reaction rates according to Eq. (21).

4. Calculate the isotopic concentrations and mass of gas in each beryllium reflector region after an irradiation time *t* using the solutions in Section 3.1.

5. Repeat steps 1–4 for the LEU core and calculate the isotopic concentrations for the same irradiation time *t*.

6. Compare the HEU and LEU isotopic concentrations and the mass of gas after the same irradiation time *t*.

7. Steps 4–6 may be repeated for another irradiation time.

4. HEATING MODEL

The energy deposition (heating rate) throughout the beryllium reflector has several components, and typically several MCNP calculations plus some post-processing are necessary to account for them. In the approach used in this study, two MCNP calculations are necessary. One calculation is used to obtain the neutron and prompt gamma components and the other the delayed gamma components. Proper normalization is then necessary to obtain the final results.

No provision was made in this study for the beta radiation from the core. The distance from the core to the beryllium reflector is too large for beta radiation to deposit its energy in the reflector and the impact was assumed to be zero.

4.1 PROMPT RADIATION

Heating in MCNP is calculated using the F6 tallies. The MCNP user may tally heating separately for neutrons and gamma, or tally it simultaneously for the two types of radiation. In this study, tallying is performed separately to enable assessment of the relative importance of the two types of radiation.

The neutronic F6 tally accounts for the kinetic energy deposited by the fission fragments, the prompt and the delayed neutrons. The fission fragments are not transported by MCNP but their energy is deposited locally at the fission site; hence, they do not impact the heating of the beryllium. Neutrons, however, can reach the reflector and deposit their kinetic energy in beryllium. It is the F6:n tally in the beryllium regions that provides the heating due to the neutrons. The delayed neutron contribution to the energy deposition tally in beryllium is accounted for only if the nuclear data library for the emitting nuclide contains this kind of data. This is considered low impact because the magnitude of this contribution is typically less than 1% of the total kinetic energy carried by all neutrons.

For gamma energy deposition, the MCNP code only accounts for prompt radiation through the F6:p tally. The following section will discuss how the delayed component of the gamma radiation is accounted for. One component that the F6:p tally accounts for is the prompt radiation coming from rapid de-excitation of the fission fragments (within 50 nanoseconds from a fission event). The tally may also account (but not automatically) for the capture gamma, the gamma radiation that is produced when a nucleus captures a neutron. As opposed to the prompt gamma component originating in the fission fragments de-excitation, the capture gamma component originates in the de-excitation of the nuclei created by neutron absorption everywhere the neutrons can reach. For this to be accounted for in MCNP, the nuclear data library must contain the corresponding gamma-production data for the nuclide that is activated. Therefore, to obtain correct results, the user must ensure that the proper nuclear data is used.

4.2 DELAYED RADIATION

The delayed gamma radiation from the fission products is not emitted immediately; rather, it is emitted sometime after creation of the fissions products. MCNP does not account for this type of radiation; additional calculations are needed for the energy deposition from these particles to be accounted for.

One way to account for the energy deposition from delayed gamma emissions is to assess this source of radiation with the ORIGEN module of SCALE, and then use this source in a fixed-source MCNP

calculation to find the energy deposition in regions of interest. This approach was used in previous HFIR heating calculations for the redesign of the beryllium reflector [5].

The approach we adopted for the current work is different and uses a more recent approach [13] based on work at the University of Michigan [14]. The approach relies on the assumption that the delayed gamma spectrum is similar to that of the prompt gamma. In this case, tracking just the prompt gamma radiation originating from fuel fission events and scaling it appropriately allows a good approximation of the energy deposited by the delayed gamma radiation to be obtained. This tracking can be accomplished by using the MCNP biasing with the PIKMT card. If $Q_{\gamma p}$ and $Q_{\gamma d}$ are the prompt and the delayed gamma energy per fission event, respectively, then the energy deposited by the delayed gamma radiation is calculated as

$$H_{\gamma d} = \frac{Q_{\gamma d}}{Q_{\gamma p}} H_{\gamma p,PIKMT} \ , \tag{22}$$

where $H_{\gamma p,PIKMT}$ is the prompt gamma energy deposition calculated with the PIKMT card. For the $Q_{\gamma p}$ and $Q_{\gamma d}$ values, we used the ENDF/B VII.0 values for ^{235}U. This should be a good approximation because most of the fission events in the HFIR reactor take place on this isotope.

4.3 METHODOLOGY

Because the energy deposition in the beryllium reflector is primarily due to more penetrating, energetic particles that originate in the core, the results should not be very sensitive to the configuration of the control elements, as was the case for gas production. Therefore, performing just one simulation, for a given control element position, should not be as much a concern from this point of view.

The main reason for concern regarding the intra-cycle irradiation is related to the isotopic composition of the reactor core that changes between the BOC and EOC. Choosing a time in the middle of the operating cycle should alleviate this concern and provide representative results for heating in the beryllium reflector. To assess the magnitude of the effect that the simulation time chosen during the operation cycle might have upon the heating results, a comparison was performed between the heating rates at BOC and at MOC_15 for the HEU core. Figure Fig. 13 shows this region-wise energy deposition rate comparison in beryllium at BOC and at MOC_15. The difference in the axial distribution indicates that the BOC values are consistently smaller than the MOC_15 values near the midplane. This trend is further reflected in the ring-wise differences (axially integrated distributions for each ring), which show smaller BOC values, by ~3.5% in the innermost ring and by almost 7% in the outermost ring (Fig. 13 right).

The methodology for the energy deposition calculation consisted of the following steps:

1. Run MCNP simulations for the HFIR HEU configuration at 15 days into a HFIR operation cycle (MOC_15) and tally the neutron and gamma heat deposition in each region of the beryllium reflector using the F6:n and the F6:p tallies, respectively.

2. Normalize to the neutron source, Eq. (21), to obtain the energy deposition rates.

3. Run MCNP simulations for the HFIR HEU configuration at 15 days into a HFIR operating cycle (MOC_15 state) with the PIKMT biasing and tally the gamma heat deposition in each region of the beryllium reflector using F6:p tallies.

4. Normalize to the neutron source, Eq. (21), and scale by the ratio of delayed to prompt gamma Q-value, Eq. (22), to obtain the energy deposition rates for delayed gamma.

5. Add results from steps 2 and 4 to obtain the total energy deposition.

6. Repeat steps 1–5 for the LEU core.

7. Compare the HEU and LEU energy deposition rates.

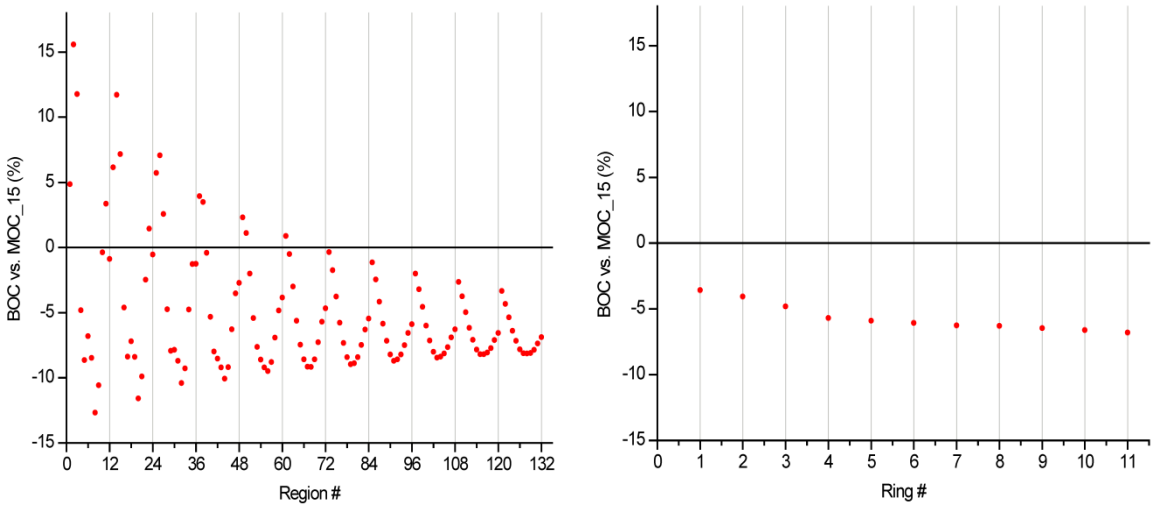

Fig. 13. Region-wise (left) and ring-wise (right) energy deposition rate comparison in beryllium for the HEU core at BOC and at MOC_15.

5. RESULTS

5.1 GAS PRODUCTION

5.1.1 Time Evolution of Gas Production

The time evolution of the gas isotopic production is observed to be close to linear for both the HEU and the LEU cores. The ^{6}Li production reaches saturation after relatively few cycles. This varies between 2 and 10 cycles, depending on the region in the reflector. FigureFig. 14 shows the time dependence for the isotopic production in two regions, both located near the HEU core midplane: region 6, located in the innermost ring of the removable reflector, and region 126, located in the outermost ring of the permanent reflector (Fig. 2). As noted, after the ^{6}Li concentration reaches saturation, the main gas production curves, for ^{4}He and ^{3}T, are nearly parallel; the ^{3}T curve is roughly one order of magnitude below the ^{4}He curve. This indicates that the production rate of the two isotopes is nearly constant with time after 10 cycles, and their fraction of the total gas production is also nearly constant with time.

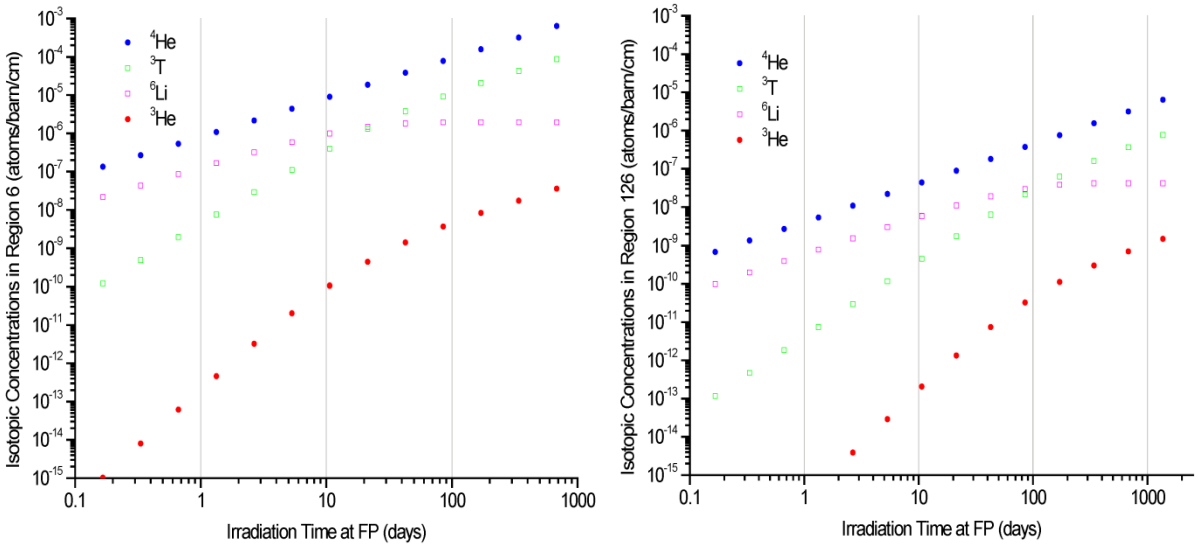

Fig. 14. Isotopic concentrations as a function of full-power irradiation time for HEU core for region 6 (left) and region 126 of the beryllium reflector.

The HEU and LEU production rates (in grams per cycle) per 25-day operation cycle after more than 10 operation cycles are shown in Table 3 for both the tritium and total gas content. It can be inferred from this table that the gas production rate in each of the reflector annuli is about 10%–12% higher with the LEU core than it is with the HEU core.

Table 3. Tritium and total gas production rates in the three reflector annuli

Reflector annulus	Tritium production rate (g/cycle)		Total gas production rate (g/cycle)	
	HEU	LEU	HEU	LEU
Removable Reflector	0.304	0.338	3.163	3.556
Semipermanent Reflector	0.075	0.083	0.773	0.865
Permanent Reflector	0.098	0.109	1.043	1.167

Table 4 shows the maximum irradiation limits (as of beginning of cycle 400) for the three annuli of the beryllium reflector, given in Reference [15]. Also shown in this table is the maximum residence time (in days and in 25-day cycles) for each annulus, assuming that the reactor operates at full power (FP) during all this time. The removable reflector was replaced before cycle 400. At that time, the other two annuli had an exposure of 36,042 MWd (about 17 cycles).

Table 4. Irradiation limits for the three reflector annuli

Reflector annulus	Irradiation limit (MWd)	FP irradiation time limit (days)	FP irradiation time limit (cycles)
Removable Reflector	83,700	985	~40
Semipermanent Reflector	167,400	1,970	~79
Permanent Reflector	279,000	3,283	~132

The total amount of gas produced in the three reflector annuli at four values of the number of cycles is given in Table 5. The 40, 79, and 132 cycles correspond approximately to the design lifetime of the removable, semi-permanent, and permanent reflectors of the HEU core, respectively, from Table 4.

With precision typically better than 1%, the relative increase in total gas production in the LEU core was independent of the irradiation time and of the reflector annulus. Table 6 shows (for 1000 days of FP irradiation) that the increase is 12–13% for each of the reflector annuli. The tritium production in the LEU core is ~11% higher than in the HEU core.

Table 5. Mass of gas produced in the three types of reflector as a function of the number of irradiation cycles for the HEU core

Reflector annulus	Mass of gas (grams)			
	17 cycles	40 cycles	79 cycles	132 cycles
Removable	53.2	125.9		
Semipermanent	13.0	30.8	60.9	
Permanent	17.4	41.4	82.1	137.4

Table 6. Increase in the mass of gas produced in the LEU core vs HEU core after 1000 days of irradiation (~40 HEU cycles)

Reflector annulus	Increase in LEU vs HEU
Removable	12.44%
Semipermanent	11.85%
Permanent	11.98%

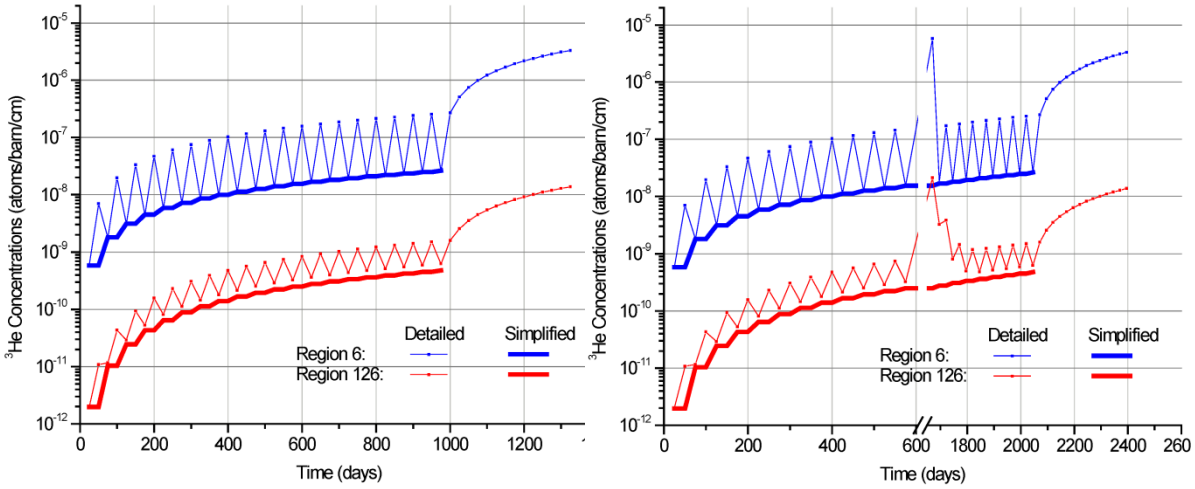

Fig. 15. Comparison of ^{3}He concentrations from HEU detailed and simplified simulations in two beryllium regions near midplane. The plot on the right has a 3-year downtime between cycles 12 and 13.

As discussed previously, the evolution in time of the isotopic concentrations does not depend on the model chosen with the noticeable exception of the ^3He concentration, which is more sensitive to the choice of a continuous or a detailed irradiation model. FigureFig. 15 shows a comparison between simulations with the detailed and simplified models for two regions near midplane, one situated closest to the reactor core (region 6) and the other furthest (region 126). The detailed simulation was performed for 20 cycles with uniform 25-day downtime between cycles and after the 20th cycle with a 300-day downtime (Fig. 15 left). The simplified model results follow the results from the detailed simulation fairly closely. One important observation is that this is also valid when a longer downtime period is allowed at some point, and the usual pattern (25 day cycle and 25 day downtime) follows again after that. In Fig. 15 (right), a 3-year downtime was introduced following cycle 12. It is noticed that after a transition period that can last a few cycles (one cycle for region 6 and approximately four cycles for region 126), the behavior becomes similar to the case illustrated in Fig. 15 (left), because the "excess" ^3He is burned quickly.

Another important conclusion from Fig. 15 is that the ^{3}He concentration can increase significantly during periods of downtime: it increases over two orders of magnitude for regions close to the core within less than 1 year of downtime (a one-order-of-magnitude increase occurs during the first 25 days, and more than one order of magnitude in about 6 months in the outermost region at the midplane).

5.1.2 Spatial Distribution of Gas Production

The gas production varies substantially as a function of the position in the beryllium reflector. It varies by approximately three orders of magnitude between the midplane regions of the innermost ring in the removable beryllium and the top or bottom regions in the outermost ring of the permanent reflector for production of both ^{3}T and ^{4}He. The axial distribution of the production of these isotopes is parabolic in the rings closest to the core and tends to become a "hat" function in the outer rings. In each ring, the maximum production is always near the midplane.

The above statements for the production of the main gaseous products do not hold for the production of ^{6}Li and ^{3}He. This is because of their sensitivities to the thermal neutron flux, and hence to the position of the control elements during the operation cycle. Their axial distribution is in general flatter than for the ^{3}T and ^{4}He, and, for the innermost rings, the maxima for these distributions is not near the reflector's midplane. The region-wise maximum-to-minimum ratios are ~100, an overall variation of only two orders of magnitude as opposed to three orders of magnitude for the main gaseous isotopes. The reason for this smoother overall behavior stems not only from the flatter axial distribution mentioned above, but also from the shallower decrease with the radial depth in the reflector.

The above discussion is illustrated in Fig. 16, which presents the number of atoms of each isotopic species per atom of beryllium at three times, corresponding to the exposure limit (Table 4) for each of the three reflector annuli.

The three-dimensional distribution and corresponding contour plot for the total gas production (mg/cm^3) are shown in Fig. 17 for 17 full power irradiation cycles with the HEU core.

The spatial distribution of the differences in LEU vs HEU region-wise gas production is not as symmetric as the gas production distribution in the HEU core, as illustrated in Fig. 18. The main gaseous components, ^{4}He and ^{3}T, show similar behavior with a higher increase at the top of the LEU core than for the bottom of the core. The asymmetric axial behavior for this difference is attributed to the particularity of the axial grading for the LEU fuel design, which reduces the amount of fuel for the bottom 3 cm of the fuel elements (Fig. 19).

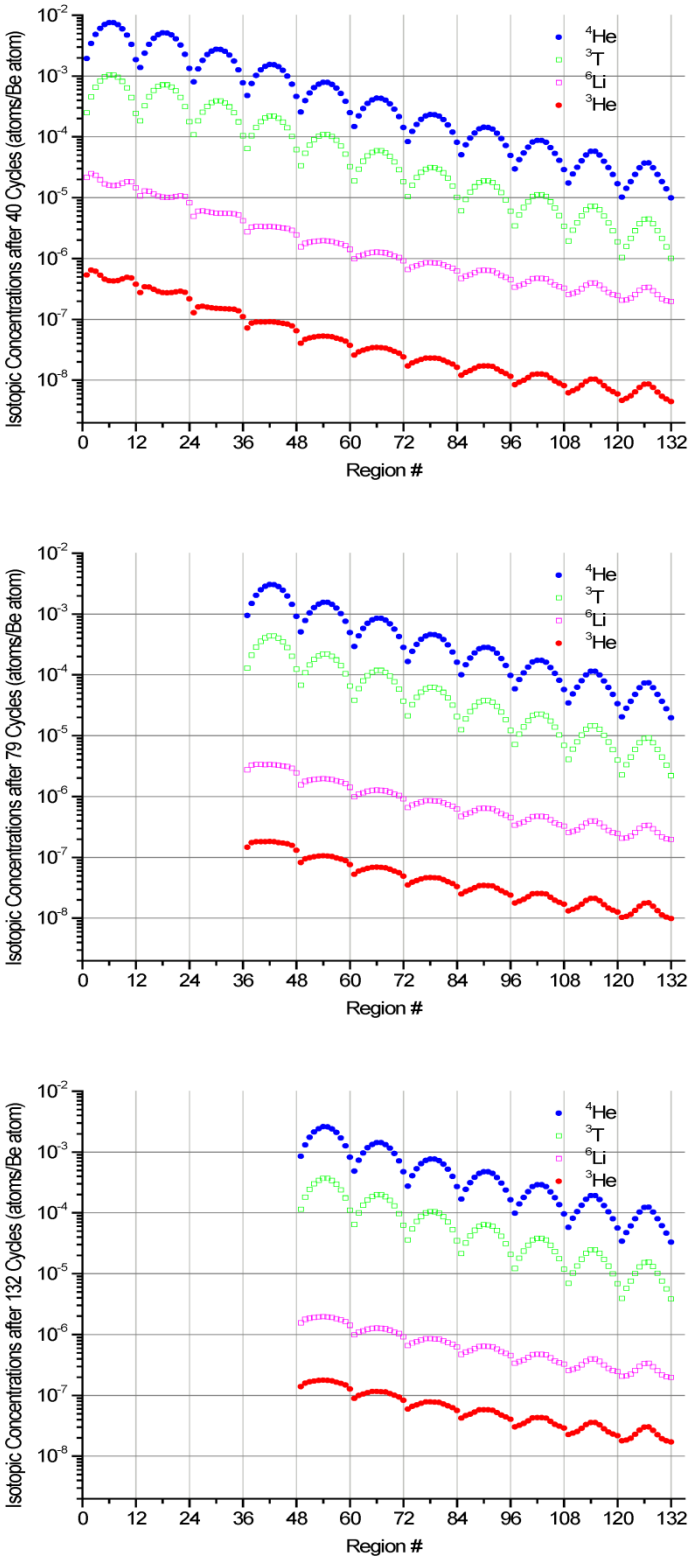

Fig. 16. Isotopic concentrations for the three beryllium annuli at exposure limit for the HEU core.

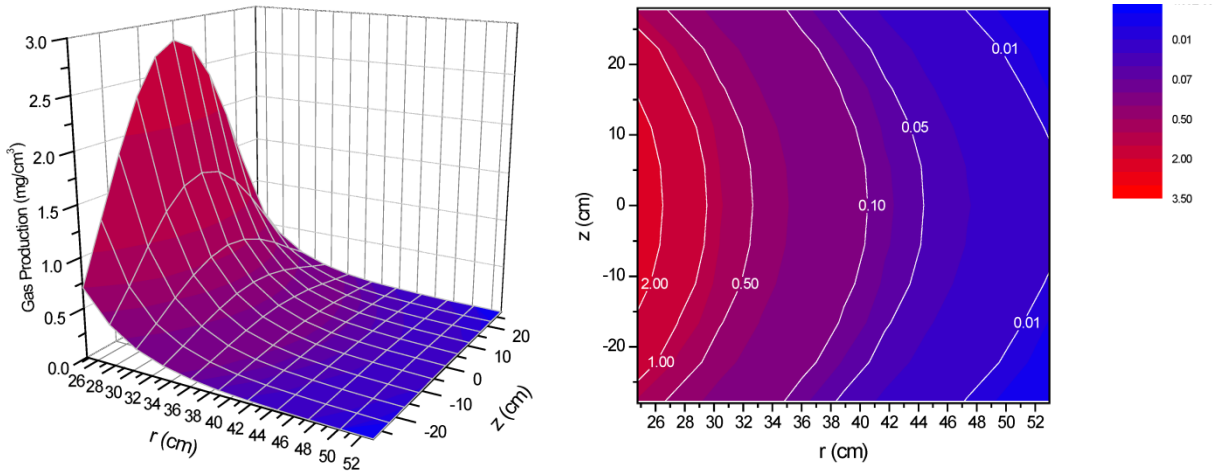

Fig. 17. Three-dimensional (left) and contour plots for the distribution of gas production in the beryllium reflector for HEU core.

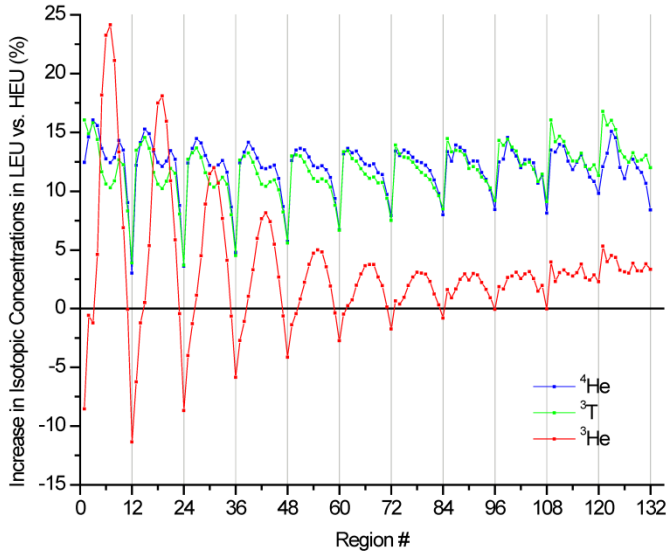

Fig. 18. Increase in region-wise isotopic gas production for the LEU core compared to HEU.

The largest variation between the LEU and HEU results for the spatial distributions is seen in the production of the ^{3}He isotope. The axial distribution of this difference is more symmetric with respect to the midplane. This behavior is likely due to sensitivity of the ^{3}He production to the thermal flux spatial distribution in the reflector, which, in turn, is due to the opening of the control elements.

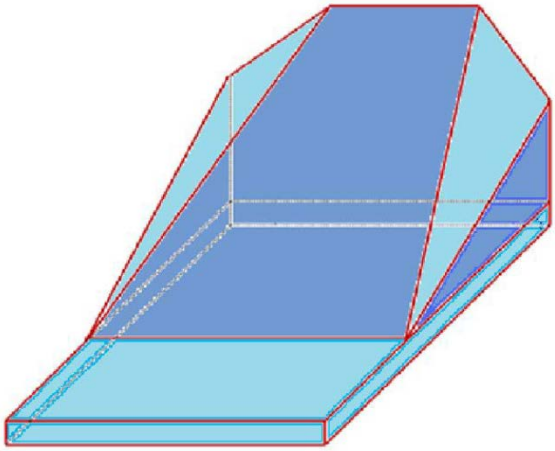

Fig. 19. Axial grading of the bottom 3 cm for the LEU fuel elements (from [1]).

5.1.3 Comparison to Previous Gas Production Studies

The midplane ^{6}Li concentrations at equilibrium obtained in this study have been compared to those obtained in previous studies, in particular those in Reference [5]. Those studies, performed in 1995, used a BOC, fresh fuel model for the HFIR core, but the control elements were positioned at a cycle-averaged height of 22 in. The equilibrium concentration obtained in our current study for the innermost reflector region (region 6) is ~1.7×10^{-5} atoms of ^{6}Li per atom of *Be*; this compares well with the previous study. However, our result for the outermost region (region 126) is ~3.4×10^{-7} atoms of ^{6}Li per atom of *Be*, about twice the value in Reference [5]. The same trend is seen for the ^{3}He concentrations: after 40 cycles of irradiation, the ^{3}He concentration we calculate is ~4.3×10^{-7} atoms of ^{3}He per atom of *Be* now vs almost 4.0×10^{-7} previously obtained for region 6, and ~8.6×10^{-9} atoms of ^{3}He per atom of *Be* now vs slightly more than 3.0×10^{-9} previously for region 126.

These results for both the neutronic poisons and the main gas production constituents calculated in the present study also show more pronounced axial variation in concentrations than previously computed in Reference [5].

The rate of tritium production computed in the present study for the HEU core is larger by 8.5% for the removable reflector and by 22.5% for permanent reflector compared to the previous studies [5]. A rate of 0.304 g/cycle for the RB reflector was computed vs a previous rate of 0.28 g/cycle, and a rate of 0.098 g/cycle was computed for the PB reflector vs a previous rate of 0.08 g/cycle.

The impact on the reactivity of the maximum poisoned model seems to be minimal for the HEU core: 100 pcm of negative reactivity, with k_{eff} decreasing from 0.99757±0.00007 for the standard cycle 400 model to 0.99656±0.00006 for the maximum poisoned model. Reference [5] reports a negative reactivity insertion due to beryllium poisoning of 300±100 pcm.

For a comparison with more recent results, the total amount of gas from each isotope produced in the beryllium reflector was calculated after 21 cycles of irradiation and it was found that the amounts of ^{3}T, ^{3}He, and ^{4}He are, respectively, 9.57, 0.00621, and 94.0 g. These results, especially for the ^{3}He, compare well with the results shown in Fig. 6 of Reference [7].

5.1.4 Impact of Gamma Radiation on Gas Production

The results presented and discussed so far neglect gas production by gamma radiation. As discussed in Section 3.6, it is possible that the gamma-induced gas production is somewhat more significant than previously thought in the PB reflector.

Estimating the gamma contribution to gas production is hindered by the fact that the corresponding reaction rate for this gamma-induced reaction cannot be obtained by a simple tally card in the MCNP input. To overcome this problem, the gamma spectrum was tallied in 238 groups using MCNP and then was manually integrated with the cross section for this reaction to obtain the reaction rate. This calculation was performed for a few regions in the permanent reflector near the midplane. The effect of delayed gammas was taken into account by doubling the prompt gamma flux, which represents an overestimation, as the delayed gamma spectrum is in reality softer than the prompt one. Therefore, the increase in the production results such as those calculated represents an upper bound for the real results. A lower bound for the gamma impact can be obtained by simply neglecting the delayed gamma component; this results in an increase of only about half the one presented below.

Gas concentrations recalculated using this approximation for the gamma-induced production indicate that the gamma radiation can add ~3.4% in ^{4}He production at the midplane of the innermost shell in the permanent reflector (region 54) and as much as ~23% in the outermost region of the reflector near midplane (region 126). FigureFig. 20 shows an almost linear dependence of the relative increase in each radial region of the permanent reflector near the midplane. Because most of the gas is generated in the inner regions, the total increase in the mass of gas generated by gamma radiation throughout the permanent reflector should be dominated by the increase in the inner, axially central regions (such as region 54) and to a lesser extent by the increase in the outer regions.

The relative increase in gas production due to gamma radiation in the LEU core is expected to be lower than that for the HEU core, based on the lower gamma contribution to the heating for this core.

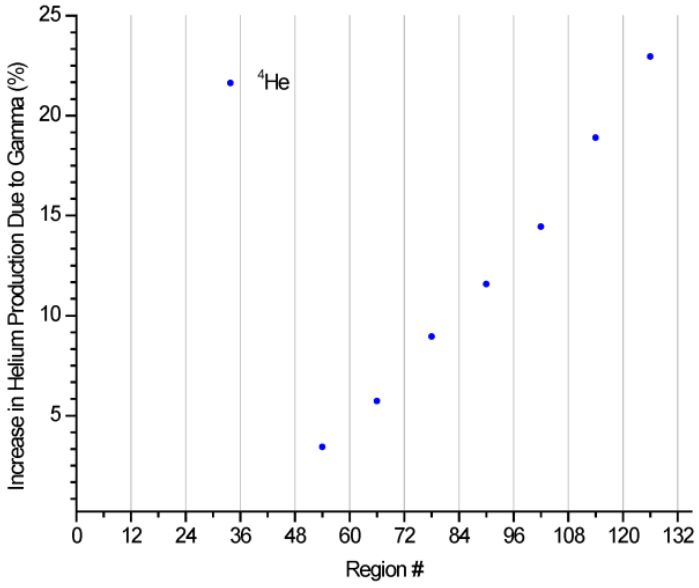

Fig. 20. Increase in helium production due to gamma radiation in the midplane regions of the permanent beryllium reflector with HEU core.

5.2 HEATING

5.2.1 Heating Results for the HEU Core

As mentioned in Section 4, the heating calculations for each region have been performed using a middle of cycle time (15 days into the operating cycle, MOC_15). Choosing this time in the cycle as a representative time for the entire cycle is more conservative, as demonstrated in Fig. 13, than previous heating calculations [5] performed with fresh fuel and control elements withdrawn at 22 in. The heating rate results at MOC_15 are interpreted to be the average heating rate for the entire cycle.

The heating was tallied on the same spatial mesh used for the gas production. In Fig. 21, the total heating rate in units of watts per gram of beryllium, per megawatt of reactor power is shown for each region in the reflector for the HEU core.

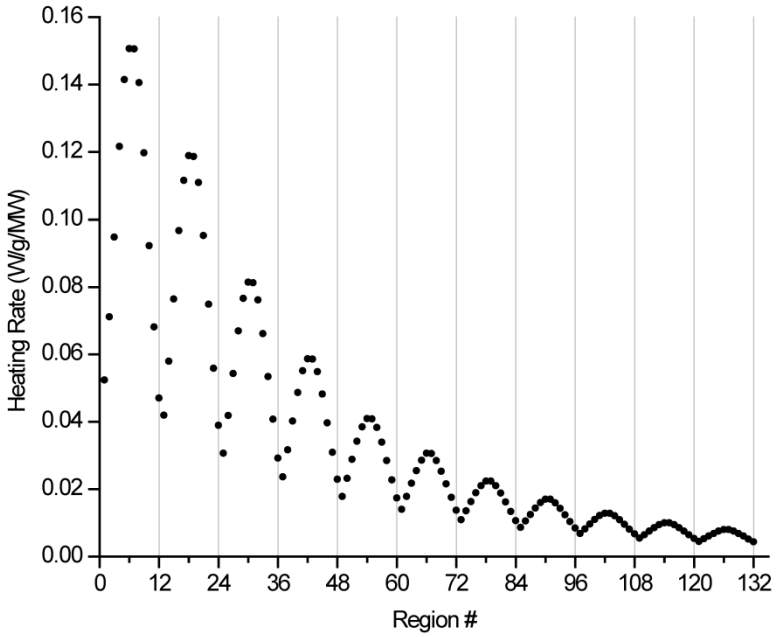

Fig. 21. Heating rate in HFIR's beryllium reflector for HEU core.

The contribution of each energy deposition component is shown in Fig. 22. The left plot of this figure shows the absolute contribution, and the right plot shows the relative contribution for each component. The prompt and capture gamma components, together labeled as "Prompt γ", constitute the main contribution in each region, which almost always is more than 50% of the total. This component's contribution increases radially at the expense of the neutronic contribution. The delayed gamma contribution is almost spatially flat at around 20% throughout the reflector and represents a greater contribution than the neutronic component for the permanent reflector.

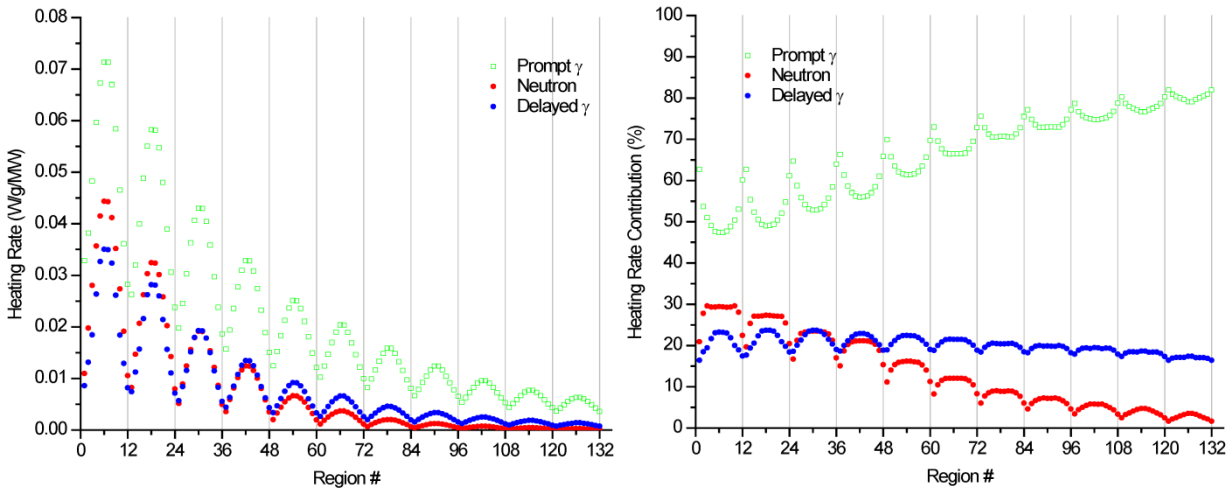

Fig. 22. Contribution of each component to the heating rate in beryllium reflector for the HEU core.

5.2.2 Heating in LEU Core and Comparisons LEU-HEU for Heating Results

The total heating rates and the heating rates by component in the beryllium reflector are shown on the left in Fig. 23 on a per MW of reactor power basis, while the contribution of each component is shown on the right. The neutronic contribution increases in the removable reflector as compared to the HEU core, and the contribution of the delayed gamma radiation to heating decreases to ~15%.

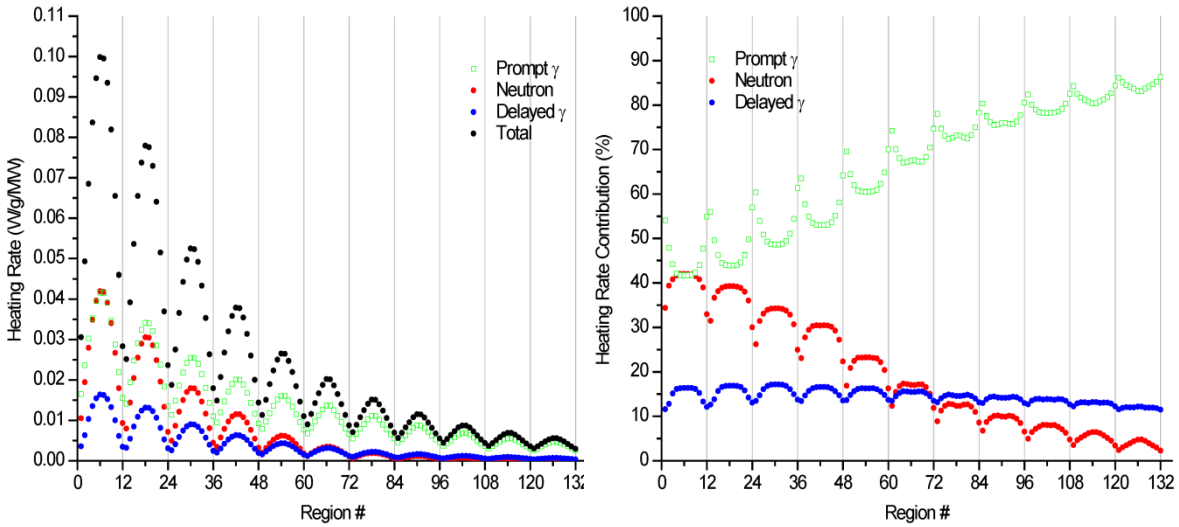

Fig. 23. Heating rate and component contribution in beryllium reflector for the LEU core.

A comparison of heat generation rates in the beryllium reflector with the LEU core shows that the total heating rate with LEU decreases by about 30–35% on a “per MW” basis (Fig. 24 left). Taking into account that the nominal power for the HFIR configuration with LEU fuel is 100 MW, compared to 85 MW for the current HEU configuration, the nominal heating rate in the beryllium reflector with the LEU core is expected to be about 20–25% lower than with HEU core (Fig. 24 right). By component, the largest decrease occurs in the gamma radiation, with the LEU delayed gamma component being only half the value of the corresponding HEU component on a per MW basis. The neutronic component decreases slightly for the LEU core on a per MW basis, but the increase in the nominal power leads to an effective increase of 10–15% in nominal terms for the neutronic component. The change in heating rate is fairly uniform across the beryllium reflector, with the notable exception of the prompt and capture gamma component, which shows a slight increasing trend radially. The decrease of the gamma heating in beryllium for the LEU case may be attributed to the increase in uranium loading, which provides more self-shielding for the gamma radiation generated in the core.

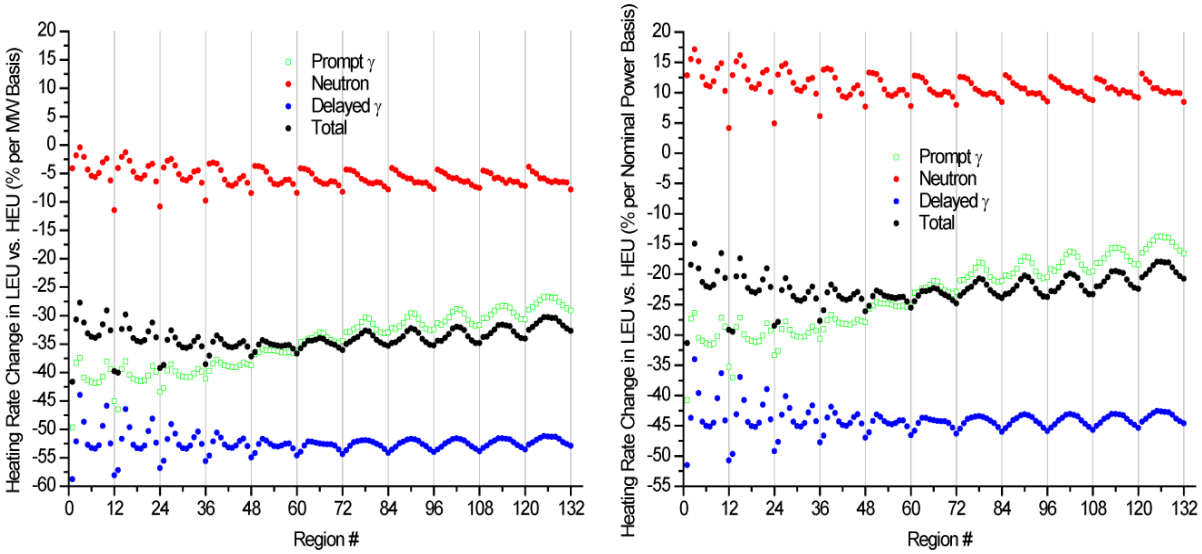

Fig. 24. LEU vs. HEU heating rate change in beryllium reflector.

5.2.3 Comparison to Previous Heating Results

Previously, in 1995, heating calculations were performed for the redesign of the HFIR beryllium permanent reflector [5]. The 1995 calculations reported results for the HEU core with fresh fuel and control elements at 22 in. withdrawn on the same radial mesh but on an axial mesh made up of only seven zones, as shown in Table 7.

Table 7. Boundaries of the zones in the beryllium reflector MCNP model of 1995 redesign study (from [5])

Zone #	Z_{top} (cm)	Z_{bottom} (cm)
1	30.48	19
2	19	11
3	11	3
4	3	-3
5	-3	-11
6	-11	-19
7	-19	-30.48

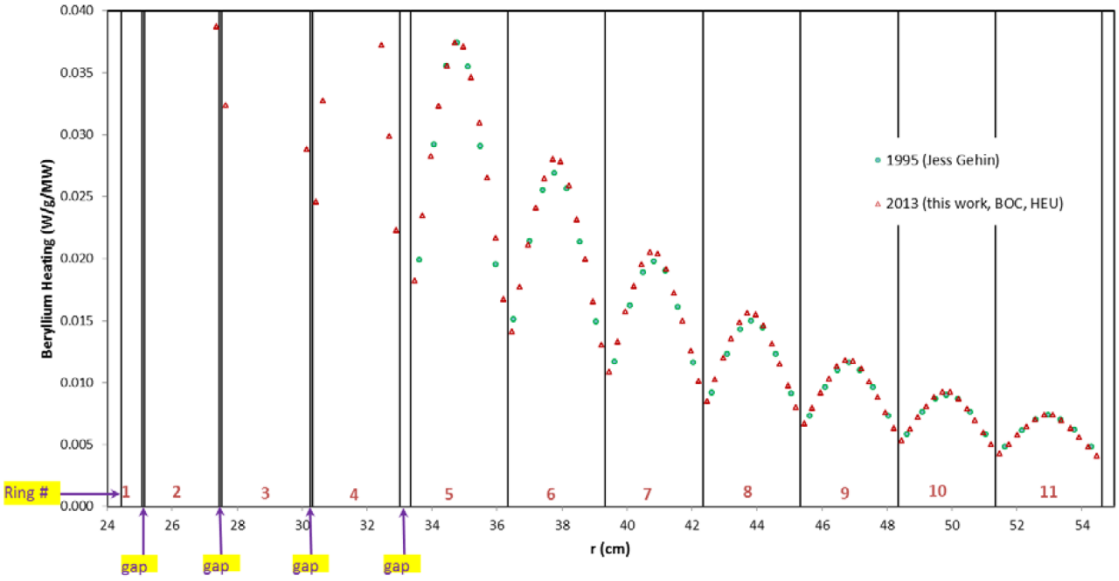

Fig. 25. Comparison of heating results for permanent reflector.

The 1995 heating results for the permanent reflector were compared with the results obtained with the current methodology for the HEU core at BOC, as shown in Fig. 25. The abscissa represents the real radial dimension for the ring. Inside each ring, the axial data is scaled to fit the width of the respective radial mesh, and the axial data points are appropriately positioned based on axial zones defined in each study. This modification in the way results are plotted was necessary to accommodate the different meshing used in the two evaluations. The comparison reveals slight underestimation in the 1995 results compared with the current results at the midplane, but the overall agreement is excellent. No heating results were reported for the removable and semipermanent reflector annuli in the 1995 study.

6. CONCLUSIONS

A systematic study of the changes in degradation factors for the beryllium reflector in HFIR with the LEU core has been performed, and comparisons with the results obtained for the current HEU core are reported. Both the LEU and HEU results have been obtained using fuel-homogenized MCNP models based on the 2011 model for the LEU core [1] and the enhanced Cycle 400 HEU model of the HFIR fresh core [1]. These models were further modified to obtain detailed distributions of the quantities of interest for this study.

The beryllium degradation factors that were analyzed were total gas production, tritium production, neutronic poison production, and the heating rate. In general, the results were reported as R-Z spatial distributions on a 132-region mesh in the beryllium reflector. The behavior of the gas, tritium, and neutronic poison production over time was also analyzed.

This study documents an extensive series of sensitivity studies that were performed to understand the range of variation in the results due to different approximations during the computational process. As a result of these analyses, a methodology was developed for calculating gas and neutron poison production. The new methodology accounts for the geometry and isotopic composition changes in the HFIR reactor during an irradiation cycle by using time-averaged reaction rates over the reactor cycle.

The results for both the HEU and LEU cores show a steep radial gradient in the gas production in the beryllium reflector. Comparison with previous studies conducted on the HEU core showed differences in both the overall production rates of gas and neutronic poisons and in the spatial distribution of the production of these isotopes. Of particular note, the axial behavior of these distributions revealed a larger variation than previously reported [5].

Comparison of gas production in beryllium with the HEU and LEU cores showed an increase of ~12% in the LEU case, but this increase was not axially uniform. Increases of up to ~17% were observed for regions at the top of the reflector and only ~3% in regions at the bottom for the main gaseous products. We attribute this asymmetry in the results to the axial contouring of the fuel in the LEU design.

Tritium production typically accounts for ~10% of the total gas production, with the balance made up of helium for both the HEU and LEU cores. The ^{3}He product, also gaseous, is negligible in the balance of total gas produced in either the HEU or LEU configurations but may be very important as a neutronic poison, especially after long periods of downtime when its concentration can increase as much as 100-fold. Similar to the gas products, the LEU core also produced a higher concentration of neutronic poisons over the same operating time. The increase was more pronounced in regions closer to the core (removable reflector) and around the midplane.

An estimate of gas production caused by gamma radiation showed that this radiation could add a few percent to the total amount of helium produced in the permanent reflector of the HEU configuration. Based on the results for gamma heating in the LEU configuration, the gamma contribution to gas production in the permanent reflector may be less for this configuration.

The heating rate in the beryllium reflector was lower in the LEU configuration than in the HEU configuration, even when taking into account the higher nominal power in the LEU configuration. Although the decrease in the neutron heating was negligible on a per-MW-of-core-power basis, and could even lead to an increase of ~10% when the nominal powers of the two configurations are accounted for, the gamma heating could be substantial. The most dramatic decrease in the heating

was seen for the heating produced by delayed gamma, which decreased by almost 50% with the LEU core when compared with the HEU configuration. Accounting for the different nominal powers of the two HFIR configurations, the overall heating rate in the beryllium reflector decreased by ~20% for the LEU core.

7. REFERENCES

1. G. Ilas and R. T. Primm, III, *Low Enriched Uranium Fuel Design with Two-Dimensional Grading for the High Flux Isotope Reactor*, ORNL/TM-2010/318, Oak Ridge National Laboratory, Oak Ridge, TN, 2011.

2. D. Ilas, *Impact of HFIR LEU Conversion on Spectral Characteristics of Experimental Locations*, LTR-2012-414, Oak Ridge National Laboratory, Oak Ridge, TN, 2012.

3. J. M. Beeston, L. G. Miller, E. L. Wood, Jr., and R. W. Moir, "Comparison of Compression Properties and Swelling of Beryllium Irradiated at Various Temperatures," *Journal of Nuclear Materials*, **122–123**, 802–809 (1984).

4 . L. Sannen, C. De Raedt, F. Moons, and Y. Yao, "Helium Content and Induced Swelling of Neutron Irradiated in Beryllium," *Fusion Engineering and Design*, **29**, 470–474 (1994).

5. S. J. Chang, J. C. Gehin, P. C. Hambaugh, R. B. Rothrock, and L. A. Smith, *High Flux Isotope Reactor (HFIR) Permanent Reflector Redesign Study*, ORNL/RRD/INT-107, Oak Ridge National Laboratory, Oak Ridge, TN, 1995.

6 . D. Chandler, R.T. Primm, III, and G.I. Maldonado, *Reactivity Accountability Attributed to Beryllium Reflector Poisons in the High Flux Isotope Reactor*, ORNL/TM-2009/188, Oak Ridge National Laboratory, Oak Ridge, TN, 2009.

7. D. Chandler, G. Maldonado, L. Proctor, and R. T. Primm, III, "Nuclear Transmutations in HFIR's Beryllium Reflector and Their Impact on Reactor Operation and Reflector Disposal," *Nuclear Technology*, **177**(3), 395–412 (2012).

8. *SCALE: A Comprehensive Modeling and Simulation Suite for Nuclear Safety Analysis and Design*, ORNL/TM-2005/39, Version 6.1, June 2011 (Available from Radiation Safety Information Computational Center at Oak Ridge National Laboratory as CCC-785.), Oak Ridge, TN, 2011.

9. N. Xoubi and R. T. Primm, III, *Modeling of the High Flux Isotope Reactor Cycle 400*, ORNL/TM-2004/251, Oak Ridge National Laboratory, Oak Ridge, TN (2005).

10. X.-5. M. C. Team, *MCNP—A General Monte Carlo N-Particle Transport Code, Version 5*, LA-CP-03-0245, Los Alamos National Laboratory, Los Alamos, NM, 2003.

11. W. Haeck, *Vesta User's Manual-Version 2.0.0*, IRSN DSU/SEC/T/2008-331-Index A, Institut de Radioprotection et de Surete Nucleaire, France, 2009.

12. D. Ilas, *Development of a SCALE Model for High Flux Isotope Reactor Cycle 400*, ORNL/TM-2011/367, Oak Ridge National Laboratory, Oak Ridge, TN, 2012.

13. J. Peterson and G. Ilas, "Calculation of Heating Values for the High Flux Isotope Reactor," *Proceedings of PHYSOR 2012 – Advances in Reactor Physics – Linking Research, Industry, and Education*, Knoxville, TN, April 15-20, 2012.

14. F. B. Brown, W. R. Martin, and R. D. Mosteller, "Monte Carlo - Advances and Challanges," (workshop presentation at PHYSOR 2008, Interlaken, Switzerland), LA-UR-08-05891, Los Alamos National Laboratory, Los Alamos, NM, 2008.

15. B. H. Cupp, “Major HFIR Components, Accumulated Megawatt-Days (MWd) at Beginning of Cycle 400 - REV. 1,” Letter from B. H. Cupp to D. J. Newland, Oak Ridge, TN, Oak Ridge National Laboratory, May 10, 2004.